



AFRL-RX-WP-TM-2013-0084

QUANTUM CONFINED SEMICONDUCTORS - In-House Interim Research

**Gail J. Brown
AFRL/RXAN**

**APRIL 2013
Interim Report**

Approved for public release; distribution unlimited.

See additional restrictions described on inside pages

STINFO COPY

**AIR FORCE RESEARCH LABORATORY
MATERIALS AND MANUFACTURING DIRECTORATE
WRIGHT-PATTERSON AIR FORCE BASE, OH 45433-7750
AIR FORCE MATERIEL COMMAND
UNITED STATES AIR FORCE**

NOTICE AND SIGNATURE PAGE

Using Government drawings, specifications, or other data included in this document for any purpose other than Government procurement does not in any way obligate the U.S. Government. The fact that the Government formulated or supplied the drawings, specifications, or other data does not license the holder or any other person or corporation; or convey any rights or permission to manufacture, use, or sell any patented invention that may relate to them.

Qualified requestors may obtain copies of this report from the Defense Technical Information Center (DTIC) (<http://www.dtic.mil>)

AFRL-RX-WP-TM-2013-0084 HAS BEEN REVIEWED AND IS APPROVED FOR PUBLICATION IN ACCORDANCE WITH ASSIGNED DISTRIBUTION STATEMENT.

//SIGNED//
GAIL J. BROWN, Program Manager
Nanoelectronic Materials Branch
Functional Materials Division

//SIGNED//
DIANA M. CARLIN, Chief
Nanoelectronic Materials Branch
Functional Materials Division

//SIGNED//
KAREN R. OLSON, Deputy Chief
Functional Materials Division
Materials & Manufacturing Directorate

This report is published in the interest of scientific and technical information exchange and its publication does not constitute the Government's approval or disapproval of its ideas or findings.

REPORT DOCUMENTATION PAGE				Form Approved OMB No. 0704-0188	
<p>The public reporting burden for this collection of information is estimated to average 1 hour per response, including the time for reviewing instructions, searching existing data sources, gathering and maintaining the data needed, and completing and reviewing the collection of information. Send comments regarding this burden estimate or any other aspect of this collection of information, including suggestions for reducing this burden, to Department of Defense, Washington Headquarters Services, Directorate for Information Operations and Reports (0704-0188), 1215 Jefferson Davis Highway, Suite 1204, Arlington, VA 22202-4302. Respondents should be aware that notwithstanding any other provision of law, no person shall be subject to any penalty for failing to comply with a collection of information if it does not display a currently valid OMB control number. PLEASE DO NOT RETURN YOUR FORM TO THE ABOVE ADDRESS.</p>					
1. REPORT DATE (DD-MM-YY) April 2013		2. REPORT TYPE Interim		3. DATES COVERED (From - To) 8 June 2011 – 8 March 2013	
4. TITLE AND SUBTITLE QUANTUM CONFINED SEMICONDUCTORS – In-House Interim Research				5a. CONTRACT NUMBER In-House	
				5b. GRANT NUMBER	
				5c. PROGRAM ELEMENT NUMBER 61102F	
6. AUTHOR(S) Gail J. Brown				5d. PROJECT NUMBER 2305	
				5e. TASK NUMBER 00	
				5f. WORK UNIT NUMBER X091 (PS113200)	
7. PERFORMING ORGANIZATION NAME(S) AND ADDRESS(ES) AFRL/RXAN 3005 Hobson Way Wright-Patterson AFB, OH 45433				8. PERFORMING ORGANIZATION REPORT NUMBER	
9. SPONSORING/MONITORING AGENCY NAME(S) AND ADDRESS(ES) Air Force Research Laboratory Materials and Manufacturing Directorate Wright-Patterson Air Force Base, OH 45433-7750 Air Force Materiel Command United States Air Force				10. SPONSORING/MONITORING AGENCY ACRONYM(S) AFRL/RXAN	
				11. SPONSORING/MONITORING AGENCY REPORT NUMBER(S) AFRL-RX-WP-TM-2013-0084	
12. DISTRIBUTION/AVAILABILITY STATEMENT Approved for public release; distribution is unlimited.					
13. SUPPLEMENTARY NOTES Approved by 88ABW Public Affairs Office: Case number 88ABW-2013-2584 on 03 JUN 2013. Report contains color.					
14. ABSTRACT This research effort involved studies on chemically synthesized quantum dots, epitaxially created quantum dots and graphene thin films. For this report we have gathered together seven research papers on chemically synthesized quantum dots that were published in the last two years. Titles are: "Analysis of Thermal Band Gap Variations of PbS Quantum Dots by Fourier Transform Transmission and Emission Spectroscopy;" "Supercritical Fluid Deposition of Uniform PbS Nanoparticle Films for Energy-Transfer Studies;" "Lead Sulfide Quantum Dot Synthesis, Deposition, and Temperature Dependence Studies of the Stokes Shift;" "Fourier Spectroscopy on PbS Quantum Dots;" "PbS Nanoparticles: Synthesis, Supercritical Fluid Deposition, and Optical Studies;" "Emission of Precipitation Deposited PbS Quantum Dots on Polyethylen Terephthalate;" "Stability Studies of Lead Sulfide Colloidal Quantum Dot Films on Glass and GaAs Substrates."					
15. SUBJECT TERMS quantum dots, graphene thin film, nanoparticles, fourier spectroscopy					
16. SECURITY CLASSIFICATION OF:			17. LIMITATION OF ABSTRACT: SAR	18. NUMBER OF PAGES 48	19a. NAME OF RESPONSIBLE PERSON (Monitor) Gail J. Brown 19b. TELEPHONE NUMBER (Include Area Code) (937) 255-9854
a. REPORT Unclassified	b. ABSTRACT Unclassified	c. THIS PAGE Unclassified			

TABLE OF CONTENTS

<u>Section</u>	<u>Page</u>
Section I. Analysis of Thermal Band Gap Variations of PbS Quantum Dots by Fourier Transform Transmission and Emission Spectroscopy.....	1
Section II. Supercritical Fluid Deposition of Uniform PbS Nanoparticle Films for Energy-Transfer Studies.....	4
Section III. Lead Sulfide Quantum Dot Synthesis, Deposition, and Temperature Dependence Studies of the Stokes Shift.....	10
Section IV. Fourier Spectroscopy on PbS Quantum Dots	16
Section V. PbS Nanoparticles: Synthesis, Supercritical Fluid Deposition, and Optical Studies	22
Section VI. Emission of Precipitation Deposited PbS Quantum Dots on Polyethylen Terephthalate.....	28
Section VII. Stability Studies of Lead Sulfide Colloidal Quantum Dot Films on Glass and GaAs Substrates.....	34
List of Acronyms, Abbreviations, and Symbols.....	44

Analysis of thermal band gap variations of PbS quantum dots by Fourier transform transmission and emission spectroscopy

B. Ullrich,^{a)} J. S. Wang, and G. J. Brown

Air Force Research Laboratory, Materials and Manufacturing Directorate, Wright Patterson AFB,
Ohio 45433-7707, USA

(Received 13 June 2011; accepted 19 July 2011; published online 22 August 2011)

Fourier transmission and emission spectroscopy was employed in the range from 5 to 300 K to measure the thermal band gap shift of 4.7 nm PbS quantum dots. The analytical comparison of fits carried out with the expressions of Varshni and Fan revealed limited accuracy of the Varshni fitting parameters. Evidence is presented that transmission spectroscopy in conjunction with the Fan model concurs with the microscopic material features, resulting in a tool to determine intrinsic properties of quantum dots. [doi:10.1063/1.3623486]

Due to their broad application potential, including telecommunications, tunable light sources, biological labeling, and photovoltaics,^{1–4} PbS quantum dots (QDs) attract ongoing research activities. Particularly, the technologically relevant thermal variation of the PbS QD photoluminescence (PL) transition was intensively studied and in absence of a specific theory, Gaponenko *et al.*⁵ raised the question whether the existing theoretical expressions for bulk band gaps can be used in order to adequately describe this specific property for QDs. By choosing this approach, some authors,^{5,6} including ourselves,⁷ found an acceptable description of the thermally induced PL peak shift, disregarding the question whether the results of the fits and the found parameters properly correlate with the intrinsic absorption properties of the QDs. With regard to the fitting models used to describe the thermal band gap variations of semiconductors the empirical Varshni⁸ equation is probably the most popular approach, while Fan⁹ derived a theoretical expression based on phonon-electron interactions. The applicability of both models has been examined for the absorption of crystalline semiconductors.¹⁰ In this paper, we used the cross-reference of PL and transmittance (TR) data in order to examine the precision of the Varshni and Fan relations for QDs. The work further demonstrates the correlation between the Debye temperature of the QDs and their thermally induced band gap dependence.

The sample was formed employing the following procedure: 70 μ L of PbS QDs (40 mg/mL, diameter (4.7 ± 0.5) nm) was added into 200 μ L of toluene solvent in a mini vial and mixed. Afterwards, in order to cover as homogeneously as possible a defined area with QDs, the mixture was dispersed on a well-cleaned glass plate, which was embedded between two teflon o-rings in a specifically designed mount of two parallel aluminum plates. The coating set for 30 min in the dark to allow the solvent to evaporate.

The PL signal was evoked with the continuous wave (cw) 532 nm emission of a frequency doubled Nd:Vanadate (Nd:YVO₄) laser, and the data were collected with a Fourier transform infrared (FTIR) BOMEM spectrometer in conjunction with an InSb detector. The actual sample temperature (5–300 K) was controlled by an optical closed cycle cryostat.

At this point, it is worthwhile to stress that the temperature dependence of the PL peak of PbS QDs is apparently not always following the expectations based on common semiconductor experience. For example, Turyanska *et al.*¹¹ reported a rather flat (≈ 0.07 meV/K) blue shift of the PL peak up to 150 K, while beyond this temperature an energy shift factor of 0.3 meV/K was observed and in another work a subtle variation of ≤ 0.1 meV/K over the temperature range ≈ 10 to 300 K was reported.¹² Encountering inconsistent PL shifts ourselves, we observed that the randomness of the results can be avoided by keeping the impinging laser intensity close to the PL threshold, because increasing the laser intensity much above the emission threshold moves the PL peak up on the energy scale—i.e., causing an extrinsic increase in the band gap (Ref. 7)—and alters the PL peak shift with temperature. The PL threshold energy is a sample specific parameter, and was found to be 5 W/cm² for the sample investigated. The measurements have been carried out by cooling the sample in the dark and by warming it up under the constant illumination.

The TR experiments were carried out employing a high resolution BOMEM spectrometer in conjunction with the InSb detector used for the PL measurements. The sample was excited with the internal global source of the BOMEM

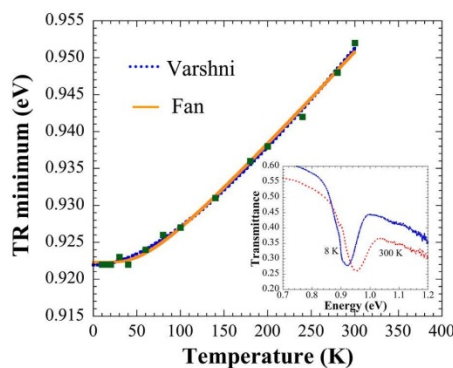


FIG. 1. (Color online) Energy of the transmittance minimum vs. temperature. The symbols represent the experimental results, and the broken and solid lines are fitted with equations of Varshni (1) and of Fan (2). The inset shows the transmittance spectra vs. energy for 8 and 300 K.

^{a)} Author to whom correspondence should be addressed. Electronic addresses: bruno.ullrich.ctr@wpafb.af.mil and bruno.ullrich@yahoo.com.

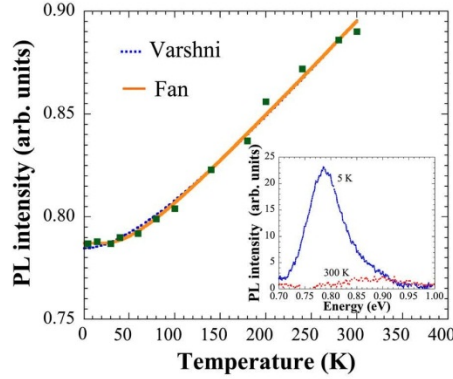


FIG. 2. (Color online) Energy of the photoluminescence peak vs. temperature. The symbols represent the experimental results, and the broken and solid lines are fitted with equations of Varshni (1) and of Fan (2). The inset shows the photoluminescence spectra vs. energy for 5 and 300 K.

while mounted in a closed-cycle optical cryostat with a temperature range of 8 to 300 K. The experiments have been carried out applying the procedure of the PL measurements.

Figures 1 and 2 show the TR minimum and PL peaks vs. temperature. Approaching 1 eV at 300 K, the TR minimum agrees reasonably with the expected band gap for ≈ 5 nm QDs. The PL peak takes place at lower energies due to the Stokes shift.⁵ The symbols represent the measurements and the dotted lines the fits for the thermal band gap dependence $E_g(T)$ according to the Varshni equation,⁸

$$E_g(T) = E_g(0) + \alpha T^2 / (\beta + T), \quad (1)$$

where $E_g(0)$ is the low limit of the band gap energy at $T=0$ K, α , and β are empiric parameters—but for several semiconductors β was found to be in reasonable agreement with the Debye temperature and α is presumed to be close to the band gap temperature coefficient ($\alpha \approx \Delta E_g / \Delta T$).^{8,10} The solid lines are the fit results using Fan's expression,^{9,10}

$$E_g(T) = E_g(0) + A / \{ \exp(\langle E_p \rangle / kT) - 1 \}, \quad (2)$$

where A is the Fan parameter, which depends on the microscopic material properties, and $\langle E_p \rangle$ is the average phonon energy responsible for the band gap variation, and $k = 8.62 \times 10^{-5}$ eV/K is the Boltzmann constant. The overall agreement of both fits with the experiment is almost identical, and the fitting parameters are summarized in Table I and II, whereas, as justified below, the Debye temperature in Table II was calculated with $\Theta_D = \langle E_p \rangle / k$. To visualize the measured spectra, the insets in Figs. 1 and 2 exhibit the TR and PL measurements at cryogenic temperatures and room temperature.

TABLE II. Fit parameters used with Eqs. (2) and (3).

Measurement	$E_g(0)$ (eV)	A (eV)	$\langle E_p \rangle$ (eV)	Θ_D (K)	S
TR	0.9223 ± 0.0003	0.0234 ± 0.0039	0.0155 ± 0.0019	180 ± 22	0.75 ± 0.22
PL	0.787 ± 0.002	0.0720 ± 0.0168	0.0132 ± 0.0024	153 ± 28	2.73 ± 1.13

TABLE I. Fit parameters used with Eq. (1).

Measurement	$E_g(0)$ (eV)	α (eV/K)	β (K)
TR	0.9219 ± 0.0003	$1.8 \times 10^{-4} \pm 2.0 \times 10^{-5}$	238 ± 58
PL	0.785 ± 0.002	$5.3 \times 10^{-4} \pm 7.1 \times 10^{-5}$	128 ± 56

Comparing the β with the Θ_D values in Tables I and II, it is apparent that the Fan equation presents the more consistent result. Nevertheless, the question is which combination of fit and measurement reveals the more accurate Θ_D , whose values are broadly scattered in the literature: (143 ± 6) K and 225 K were reported for bulk,^{13,14} while, fitting the thermal PL peak shift of QDs with the Varshni equation, β was found to be (143 ± 48) K,⁵ 75 K and 125 K.⁷ Although fairly scattered as well, these data suggest that Θ_D is below 200 K. Furthermore, the found average phonon energies of 13.2 and 15.5 meV from the PL and TR measurements in Table II agree very well with the PL fit value of (11.7 ± 1.7) meV reported by Gaponenko *et al.*⁵ who used O'Donnell's and Chen's expression,¹⁵

$$E_g(0) = E_g(0) + S \langle E_p \rangle [\coth(\langle E_p \rangle / 2kT) - 1], \quad (3)$$

where S is the Huang-Rhys factor, which is a measure of the strength of the electron-phonon coupling. We note that due to $S = A / \{ 2 \langle E_p \rangle \}$ and the identity $2 / (e^x - 1) = \coth(x/2) - 1$, Eqs. (2) and (3) are equal and a fit using either equation results in the same fitting parameters. The S values are also displayed in Table II.

Regarding our experience with laser excited PL, i.e., the possible creation of extrinsic features by the laser irradiation, we expect that TR results achieved with low light intensity are more closely related to the intrinsic properties of the QDs. In addition, energy relaxations of excited electrons into the dark exciton ground states via multi-phonon processes before radiative electron-hole recombination takes place causes a redshift—commonly called Stokes shift—of the PL peak with respect to the fundamental transition.¹⁶ This process adds an additional temperature dependent phenomenon to the band gap shift. We also note here that the overall temperature coefficient for TR and PL is quite different: 1×10^{-4} eV/K and 3×10^{-4} eV/K, reducing the Stokes shift for increasing temperatures. These additional effects influence the PL fitting parameters. In order to weigh the quality of the A parameters in Table II, it is clearly necessary to calculate the theoretically expected Fan factor, which is widely temperature invariant. The microscopic expression for A is given by^{10,17}

$$A = \frac{e^2}{\sqrt{2}\hbar} (m_0 \langle E_p \rangle)^{1/2} \frac{1}{4\pi\epsilon} \left(\frac{1}{\epsilon_\infty} - \frac{1}{\epsilon_0} \right) \left[\left(\frac{m_e}{m_0} \right)^{1/2} + \left(\frac{m_h}{m_0} \right)^{1/2} \right], \quad (4)$$

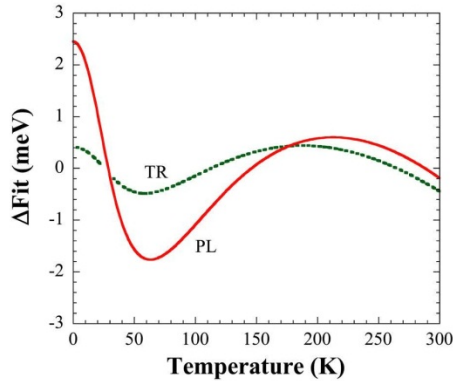


FIG. 3. (Color online) Difference between the fit done with the Fan expression (Eq. (2)) and the Varshni formula (Eq. (1)).

where e ($=1.602 \times 10^{-19}$ As) is the elementary charge, \hbar ($=1.054 \times 10^{-31}$ Js) is Planck's constant divided by 2π , m_0 ($=9.11 \times 10^{-31}$ kg) is the free electron mass, ϵ ($=8.854 \times 10^{-12}$ As/Vm) is the vacuum permittivity, ϵ_0 ($=150$) is the static, ϵ_∞ ($=16.8$) is the high frequency dielectric constant,¹⁸ and m_e ($=0.080$) and m_h ($=0.075$) are the effective electron and hole mass.¹⁹ We discuss now Eq. (4) in context with fit values in Table II. Apparently, $A_{PL}=72.0$ meV is blown out of the phonon energy range and would require the non-realistic value of $\langle E_p \rangle = 439$ meV. On the other hand, $A_{TR}=23.4$ meV corresponds to $\langle E_p \rangle = 46.4$ meV, which exceeds the expected value of 15.5 meV—corresponding to $A=13.5$ meV—but goes along with the scatter for A values fitted with Eq. (2) and calculated with Eq. (4) for crystalline materials.¹⁰ Furthermore, $S_{TR}=0.75$, rather than $S_{PL}=2.73$, is in much better agreement with the value of ≈ 0.7 for 3 nm PbS QDs.²⁰ In general, S values determined with PL fits exceed unity (1.48 in Ref. 5, and 1.34 and 1.41 in Ref. 7). Hence, by confirming our expectations, we conclude that the TR analysis reveals parameters closer to the intrinsic PbS QD features than the evaluation of PL results. However, perfect agreement between the intrinsic features of QDs and bulk cannot be expected because in the nano-regime basic properties such as heat capacity and Debye temperature are a function of size.²¹

We address now the relation between $\langle E_p \rangle$ and Θ_D . Looking at the data in Refs. 15 and 22, the relationship $\langle E_p \rangle = k\Theta_D$ holds for GaAs and GaP but not for Si and C. The reason can be deduced from the shape of $E_g(T)$, which is nonlinear for $T < \Theta_D$ due to the limited number of excited phonon modes, while at elevated temperatures, approaching and passing Θ_D , all possible phonon modes get excited and $E_g(T)$ turns into a linear dependence. Semiconductors such as GaAs and GaP, and the investigated PbS QDs, which overcome the nonlinear region of $E_g(T)$ below ≈ 250 K, show a tendency to obey $\langle E_p \rangle = k\Theta_D$. A consistency check whether the fit with Eqs. (2) and (3) reveals Θ_D can be done with the relation $\Theta_D = A/\alpha$, which holds for the linear range of $E_g(T)$. For $T \geq 140$ K the linear fit of TR(T) in Fig. 1 gives $\alpha_{TR} = 1.3 \times 10^{-4}$ eV/K (goodness of fit 0.995), resulting with $A_{TR} = 23.4$ meV from Table II in $\Theta_D = 180$ K, verify-

ing that the fit of the TR measurements reveals indeed Θ_D . With the α values of the Varshni fit in Table I, A/α gives 44 and 130 K. As found in previous works on crystalline semiconductors¹⁰ and PbSe QDs,²³ the Varshni formula overestimates α .

The goodness of fit in Figs. 1 and 2 is better than 0.996 for all fits independent of the expression used. As already mentioned, from the standpoint of the visible agreement with the experimental data both models are more or less identical. Hence, it is of interest to actually compare the difference of both fits in order to point out where and how they differ. We define ΔFit by the Fan fit minus the fit done with the Varshni relation. The result is shown in Fig. 3. Overall the TR fits reveal an improved congruent behavior (± 0.5 meV) with respect to the PL fits. At cryogenic temperatures ΔFit for the PL is more severe than at elevated temperatures because the dominating T^2 dependence at low temperatures of the Varshni relation does not properly fit the almost constant part of $E_g(T)$ below ≈ 30 K.

Summarizing, the work promotes the use of the Fan model for the theoretical description of the thermal band gap shift of PbS QDs. The presented results further advocate the measurement of absorption properties rather than emission in order to get a consistent set of data for macroscopic and microscopic parameters, such as Debye temperature and Fan factor.

This work was supported by the Air Force Office of Scientific Research (AFRL/RSE, Dr. Kitt Reinhardt).

- ¹L. Bakueva, S. Musikhin, M. A. Hines, T.-W. F. Chang, M. Tzolov, G. D. Scholes, and E. H. Sargent, *Appl. Phys. Lett.* **82**, 2895 (2003).
- ²L. Bakueva, I. Gorelikov, S. Musikhin, X. S. Zhao, E. H. Sargent, and E. Kumacheva, *Adv. Mat.* **16**, 926 (2004).
- ³J. J. Peterson and T. D. Krauss, *Nano Lett.* **6**, 510 (2006).
- ⁴K. P. Acharya, N. N. Hewa-Kasakarage, T. R. Alabi, I. Nemitz, E. Kohn, B. Ullrich, P. Anzenbacher, and M. Zamkov, *J. Phys. Chem.* **114**, 12496 (2010).
- ⁵M. S. Gaponenko, A. A. Lutich, N. A. Tolstik, A. A. Onushchenko, A. M. Malyarevich, E. P. Petrov, and K. V. Yumashev, *Phys. Rev. B* **82**, 125320 (2010).
- ⁶C. Liu, J. Heo, X. Zhang, and J.-L. Adam, *J. Non-Cryst. Solids* **354**, 618 (2008).
- ⁷B. Ullrich, X. Y. Xiao, and G. J. Brown, *J. Appl. Phys.* **108**, 013525 (2010).
- ⁸Y. P. Varshni, *Physica* **34**, 148 (1967).
- ⁹H. Y. Fan, *Phys. Rev.* **82**, 900 (1951).
- ¹⁰I. A. Vainshtein, A. F. Zatspin, and V. S. Kortov, *Phys. Solid State* **41**, 907 (1999).
- ¹¹L. Turyanska, A. Patané, M. Henini, B. Hennequin, and N. R. Thomas, *Appl. Phys. Lett.* **90**, 101913 (2007).
- ¹²W. Lü, F. Yamada, and I. Kamiya, *J. Vac. Sci. Technol. B* **28**, C5E8 (2010).
- ¹³K. G. Subhadra and D. B. Sirdeshmukh, *Pramana* **10**, 357 (1978).
- ¹⁴D. H. Parkinson and J. E. Quarrington, *Proc. Phys. Soc.* **67**, 569 (1954).
- ¹⁵K. P. O'Donnell and X. Chen, *Appl. Phys. Lett.* **58**, 2924 (1991).
- ¹⁶N. O. Dantas, P. M. N. de Paula, R. S. Silva, V. Lopez-Richard, and G. E. Marques, *J. Appl. Phys.* **109**, 024308 (2011).
- ¹⁷H. Y. Fan, *Photon-Electron Interaction: Crystals Without Fields* (Springer, Berlin, 1967).
- ¹⁸G. Guizzetti and A. Borghesi, *Handbook of Optical Constants of Solids*, edited by E. D. Palik (Academic, San Diego, 1985), Vol. 5.
- ¹⁹I. Chakraborty and S. P. Moulik, *J. Nanopart. Res.* **7**, 237 (2005).
- ²⁰T. D. Kraus and F. W. Wise, *Phys. Rev. B* **55**, 9869 (1997).
- ²¹M. X. Gu, C. Q. Sun, Z. Chen, T. C. Au Yeung, S. Li, C. M. Tan, and V. Nosik, *Phys. Rev. B* **75**, 125403 (2007).
- ²²K.-C. Chiu, Y.-C. Su, and H. A. Tu, *Jpn. J. Appl. Phys.* **37**, 6374 (1998).
- ²³A. Kigel, M. Brumer, G. I. Maikov, A. Sashchiuk, and E. Lifshitz, *Small* **5**, 1675 (2009).

Supercritical Fluid Deposition of Uniform PbS Nanoparticle Films for Energy-Transfer Studies

Joanna S. Wang,^[a] Gail J. Brown,^[a] Wei-Chun Hung,^[b] and Chien M. Wai^{*[b]}

Using supercritical fluid CO₂ (Sc-CO₂) as a medium, PbS nanoparticles can be uniformly deposited on surfaces of various substrates. Sc-CO₂ deposition of PbS nanoparticles on carbon-coated copper grids, into small holes in silicon, and formation

of uniform PbS nanoparticle films on glass are described. Fluorescence spectra of PbS nanoparticles obtained from the films prepared by the Sc-CO₂ method indicate effective energy transfer between PbS nanoparticles of different sizes.

1. Introduction

Recently, there has been much interest in the synthesis and characterization of metal sulfide semiconductor nanoparticles due to their unique optical and electronic properties.^[1–3] Metal sulfide nanoparticles have potential applications in many fields including solar cells,^[4] lasers,^[5] LED devices,^[6,7] IR detectors,^[8] telecommunication,^[9] solar absorber and photography,^[10–12] optical switches and optical amplification.^[13,14] Lead sulfide is a Group IV–VI semiconductor with a narrow direct band gap (0.41 eV) and large exciton Bohr radius of nearly 20 nm.^[15,16] These properties make PbS an interesting system for studying the effects of quantum confinement. It is known that PbS nanoparticles can provide photoluminescence over the whole transmission window (1.2–1.7 μm) of silica optical fibers and therefore, can be potentially used for universal optical amplifiers.^[17] A number of reports regarding the synthesis and characterization of PbS nanoparticles in different matrices can be found in the literature.^[18–21] Using metal sulfide quantum dot fluorophores for non-radiative energy transfer is of current interest because of its potential applications in a wide range of chemical systems.^[22] Fluorescence resonance energy transfer (FRET) involving PbS quantum dots is of special interest because the fluorescence wavelength of nanometer-sized PbS particles occurs typically in the near infrared region. FRET is sensitive to nanometer-scale changes in the donor–acceptor separation distance. Techniques of making uniform films of metal sulfide quantum dots with controllable inter-particle distances are needed for FRET studies. However, it is still a challenge to develop efficient methods of depositing PbS nanoparticles in nanostructures or making uniform films for studying their optical properties.

Supercritical fluid carbon dioxide (Sc-CO₂) is known to have a near-zero surface tension and provides an ideal medium for depositing nanoparticles in small structures or to form thin layers of ordered arrays, which cannot be achieved by traditional solvent deposition methods.^[23] For example, Smetana et al. have demonstrated that gold and platinum nanoparticles can be uniformly deposited in nanometer-sized holes ion-milled in silicon substrates and can form layers of close-packed arrays with long-range order using a Sc-CO₂ process.^[24,25] Wang

et al. have also reported the deposition of Ag₂S and CdS nanoparticles in nanostructures of semiconductor substrates using Sc-CO₂ as a medium.^[23]

In the present work, supercritical fluid deposition of PbS nanoparticles in small holes in silicon substrates and the formation of uniform PbS nanoparticle films on glass are described. Spectroscopic data of the PbS nanoparticle films and energy transfer between PbS nanoparticles of different sizes are also reported.

2. Results and Discussion

Characterization of PbS Nanoparticle Arrays

Figure 1 shows transmission electron microscopy (TEM) images of PbS nanoparticle arrays formed by the Sc-CO₂ deposition method. The average particle size (diameter) of the PbS quantum dots is 4.7 ± 0.5 nm. The average distance between two adjacent PbS nanoparticles from center to center is 7.8 ± 0.7 nm. These measurements were taken using the ImageJ software. According to Bain et al.^[26] the ligand length L [nm] can be approximated by $L = 0.25 \pm 0.127n$, where n is the number of carbon atoms in the alkyl chain.^[27–29] The equation gives a theoretical value of $L = 2.536$ nm for a single oleic acid molecule. The average values for the interparticle distance between two adjacent PbS nanoparticles stabilized by oleic acid is 3.1 ± 0.6 nm, in the two-dimensional (2D) arrays shown in

[a] Dr. J. S. Wang, Dr. G. J. Brown
Materials & Manufacturing Directorate
Air Force Research Laboratory
3005 Hobson Way, Wright-Patterson Air Force Base
OH, 45433 (USA)

[b] Dr. W.-C. Hung, Dr. C. M. Wai
Department of Chemistry
University of Idaho
Renfrew Hall Rm 116, Moscow, ID, 83844 (USA)
Fax: (+1) 208-885-6173
E-mail: cwai@uidaho.edu

Supporting information for this article is available on the WWW under <http://dx.doi.org/10.1002/cphc.201200042>.

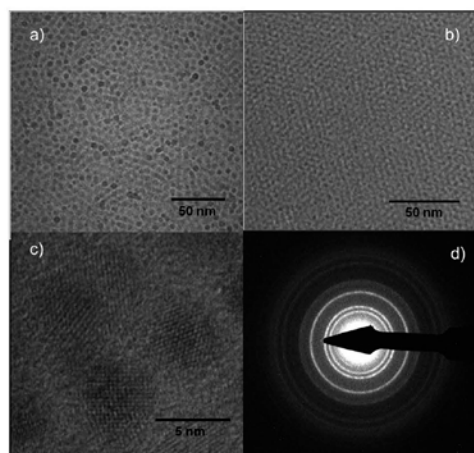


Figure 1. TEM of PbS nanoparticles deposited on copper grids in Sc-CO₂. a) PbS size 4.7 ± 0.5 nm, the average values for interparticle distance between two adjacent PbS nanoparticles stabilized by oleic acid is 3.1 ± 0.6 nm, and b) PbS size 2.3 ± 0.3 nm, the average values for interparticle distance between two adjacent PbS nanoparticles stabilized by oleic acid is 2.7 ± 0.5 nm. c) HRTEM image and d) electron diffraction of PbS nanoparticles of 4.7 nm. The conditions to prepare the particles are given in the Experimental Section.

Figure 1. The experimental values suggest an intensive interdigitation of the protecting ligands between the lead sulfide semiconductor nanoparticles due to the long alkyl chain of oleic acid. A second batch of smaller sized PbS nanoparticles was also fabricated. The size of the smaller PbS nanoparticles is 2.3 ± 0.3 nm and the average interparticle distance between the two adjacent PbS nanoparticles stabilized by oleic acid is 2.7 ± 0.5 nm. The high resolution TEM (HRTEM) image (c) in Figure 1 shows the well-formed lattice planes of the PbS nanoparticles, and the electron diffraction pattern (Figure 1 d) of the particles also indicates high crystallinity.

Benchtop solvent deposition of PbS can form arrays on the TEM copper grids immersed in the solution under atmosphere pressure (Figure 2, left). However, the benchtop solvent-evapo-

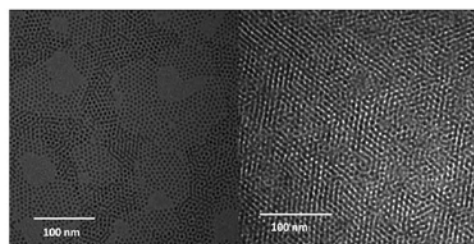


Figure 2. TEM images of PbS. Benchtop solvent deposition showing voids and uneven coverage of PbS on carbon-coated Cu grid surface (left) and supercritical fluid solution deposition showing long-range and well organized arrays (right). Size of PbS nanoparticles 4.7 ± 0.5 nm.

ration process leads to imperfect nanoparticle ordering, such as isolated islands, percolating domains, locally high particle population, and uneven surface coverage as described in the literature.^[30–33] In supercritical fluid deposition, the PbS nanoparticles show long-range order and well organized arrays (Figure 2, right).

The X-ray diffraction (XRD) pattern of the oleic acid-capped PbS nanoparticles is given in Figure 3. All diffraction peaks can be indexed to face-centered-cubic (fcc) PbS nanoparticles. The sharp peaks indicate that the product is highly crystalline. The following peaks were observed in every XRD pattern of the synthesized PbS nanoparticles: $2\theta = 25.96, 30.06, 43.06, 50.98, 53.4, 62.54, 68.88, 70.96, \text{ and } 78.92^\circ$ which correspond to the {111}, {200}, {220}, {311}, {222}, {400}, {311}, {420}, and {422} planes of the fcc structure of bulk PbS, respectively. The XRD patterns agree with standard reference data [Joint Committee on Powder Diffraction Standards (JCPDS)] for PbS galena.

Deposition of PbS Nanoparticles in Nanoscale Structures of Semiconductor Substrate

A unique feature of Sc-CO₂ as a particle deposition medium is its penetration ability. For instance, metal nanoparticles can be placed into nanostructures on a Si substrate surface by Sc-CO₂ deposition as described in a previous report.^[24] Figure 4a shows the scanning electron microscopy (SEM) image of nanoscale holes formed in the surface of a (111) oriented Si sample by ion milling using a FEI strata BD235 focused ion beam (FIB) with a 30 keV Ga⁺ ion beam. Benchtop deposition through typical solvent evaporation was achieved by placing the as-milled Si sample (4.5×4.5 mm²) in the bottom of a small glass vial filled with oleic acid-stabilized PbS nanoparticles in toluene. This process resulted in an inhomogeneous deposition with large voids in the nanostructures (Figure 4b). When the evaporation was carried out in a Sc-CO₂ cell with an as-milled Si sample placed in an environment with the same oleic acid-stabilized PbS toluene solution, the PbS nanoparticles were deposited uniformly into the nanoscale holes (Figure 4c). The nanoscale pores were packed with PbS nanoparticles filling in the available space. The details of the supercritical fluid deposition procedure to fill nanoparticles in semiconductor nanostructures are given in a previous paper.^[23]

Making PbS Nanoparticle Films on Glass in Sc-CO₂

The optical properties of the PbS nanoparticle arrays are largely unknown. Optical properties of PbS nanoparticle assemblies are of particular interest because they may lead to new materials for optical applications in the near-infrared region. For this reason, we developed methods for making uniform films of PbS nanoparticles on different substrates in Sc-CO₂ for spectroscopic studies. In our initial experiments, glass was selected as the substrate for spectroscopic investigation because it is a simple transparent insulator.

PbS nanoparticle films of different thickness were prepared using the device shown in Figure 5. The PbS nanoparticle films deposited on glass in Sc-CO₂ exhibited uniform coverage,

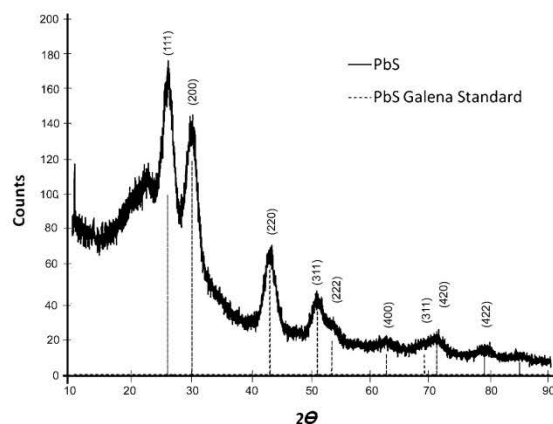


Figure 3. XRD of PbS nanoparticles.

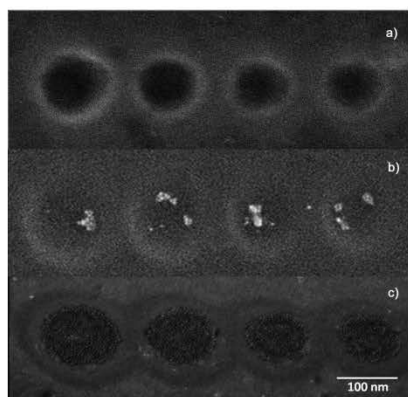


Figure 4. SEM images of a) blank holes before deposition, b) benchtop solvent deposition, and c) supercritical fluid vapor deposition of PbS into small holes in silicon.

whereas the films produced by benchtop solvent evaporation always showed rough surfaces and irregular coverage. Examples of PbS nanoparticle films formed with this device in Sc-CO_2 and in open air are shown in the Supporting Information (Figure S-1). The method to measure the film thickness was described in the Supporting Information and Figure S-2.

To view the surface morphology of the PbS nanoparticle films, we used chromium (Cr)-coated glass to prepare the films in Sc-CO_2 , following the same procedure described above for making PbS nanoparticle films on uncoated glass. The conductive nature of the Cr-coated glass allows SEM imaging of the PbS nanoparticle films. A typical SEM picture of a PbS nanoparticle film prepared by the Sc-CO_2 method is shown in Figure 6. The surface of the film is covered with well-ordered PbS nanoparticles.

Absorption and Fluorescence Spectra of PbS Nanoparticle Films

Figure 7 shows the fluorescence spectra of PbS nanoparticles (2.3 nm and 4.7 nm diameter) in toluene and after the formation of films by Sc-CO_2 deposition on glass. There is generally a small red shift of the fluorescence peak wavelength for the PbS nanoparticles condensed in the film relative to that in the toluene solution. For example, the fluorescence peak wavelength of the 2.3 nm PbS nanoparticle film is red-shifted by about 50 nm relative to that in the toluene solution (980 nm, Figure 7a). A similar but smaller red shift (about 20 nm) was also observed for the fluorescence peak of the 4.7 nm PbS nanoparticle film relative to the same PbS nanoparticle sample in toluene solution (1385 nm, Figure 7b). It should be noted that the PbS nanoparticles used in our experi-

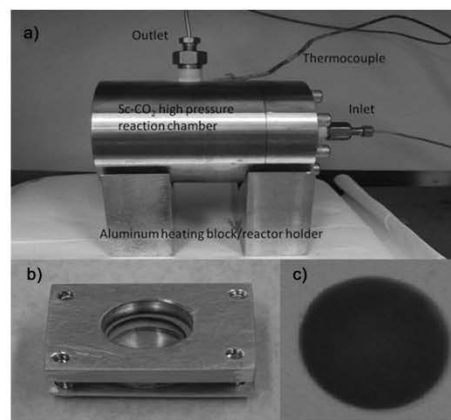


Figure 5. Apparatus for making PbS nanoparticle films on glass in Sc-CO_2 . a) High pressure reaction chamber, b) apparatus for Sc-CO_2 deposition of PbS nanoparticles on glass, and c) PbS nanoparticle film formed on glass by the Sc-CO_2 deposition method.

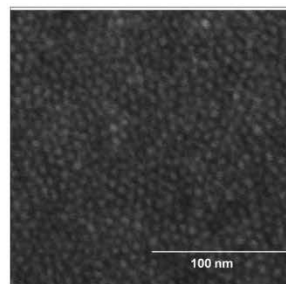


Figure 6. SEM image of surface of a PbS nanoparticle film prepared by the Sc-CO_2 deposition on a Cr coated glass.

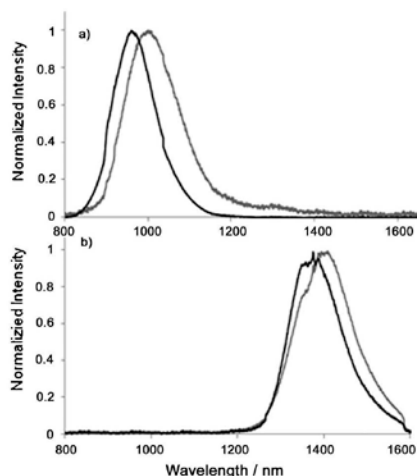


Figure 7. Overlaid fluorescence spectra of a) 2.3 nm and b) 4.7 nm PbS nanoparticles in toluene solution (black) and in film prepared by Sc-CO₂ deposition on glass (gray). Peak intensities are normalized to the maximum point as 1.0 for comparison.

ments have a size distribution in the range of 10–13%. Energy transfer may occur when two PbS nanoparticles of different sizes are in close contact in a compact film.^[34–37] This would result in a small red shift of the emission peak wavelength of PbS nanoparticles in the film relative to that in the solution as reported by Clark et al.^[38]

The absorption spectra of each group of the PbS nanoparticles (2.3 nm and 4.7 nm) in the toluene solution and in the films prepared by the Sc-CO₂ deposition method are given in Figure 8. There is no significant difference in absorption wavelength between the PbS nanoparticles in the solution and in the film for each group of the quantum dots. The absorbance maxima of PbS nanoparticles for the 2.3 nm and the 4.7 nm samples in the toluene solution and in the film are around 890 nm and 1330 nm.

The absorption spectra of a mixture of the two PbS nanoparticle solutions and the film prepared from the mixed solution using the Sc-CO₂ deposition method are given in Figure 9. Again, there are no obvious changes in either the wavelength or the relative absorbance ratio of the two PbS absorption peaks.

The fluorescence spectrum of the mixed solutions is shown at the bottom of Figure 10. Two distinct fluorescence peaks are visible from the spectrum, one centered at about 980 nm and the other at about 1385 nm, corresponding to the emission wavelengths of the 2.3 nm and the 4.7 nm PbS nanoparticles in the solution. A significant observation in this experiment is that the relative fluorescence intensities of the two peaks changed drastically for the mixed nanoparticle film formed in Sc-CO₂ (Figure 10). The initial solution has a relative fluorescence intensity ratio of about 1:1.3 for the 2.3 nm/4.7 nm PbS peaks. In the Sc-CO₂-formed PbS nanoparticle film

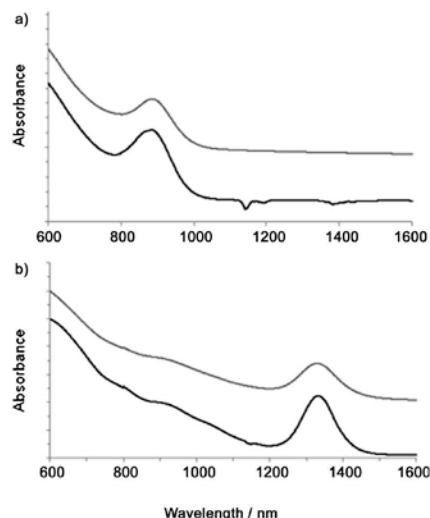


Figure 8. Overlaid absorption spectra of a) 2.3 nm and b) 4.7 nm PbS nanoparticles in toluene solution (black) and in the film prepared on glass by the Sc-CO₂ deposition method (gray).

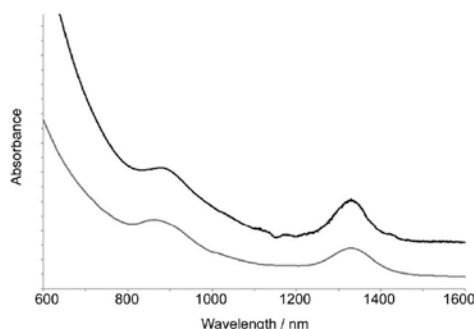


Figure 9. Absorption spectra of a mixture of the 2.3 nm and the 4.7 nm PbS nanoparticles in toluene solution (black) and a film prepared from the solution using the Sc-CO₂ deposition method (gray).

prepared from this solution, the fluorescence intensity ratio of the two peaks (2.3 nm/4.7 nm) changes to a value close to 1:8.5. Energy transfer between PbS quantum dots of different sizes obviously occurs effectively in the solid film on glass prepared by the Sc-CO₂ deposition method. Clark et al. have estimated a Förster radius of 8 nm for the PbS quantum dots fluorescence resonant energy transfer.^[38] The separation of PbS nanoparticles in the films on glass formed by the Sc-CO₂ deposition method is certainly less than the estimated Förster radius. The FRET result is reproducible for fluorescence measurements on different locations of the supercritical fluid-prepared film. It should be noted that the fluorescence ratio of the two peaks would go back to the initial value when the film

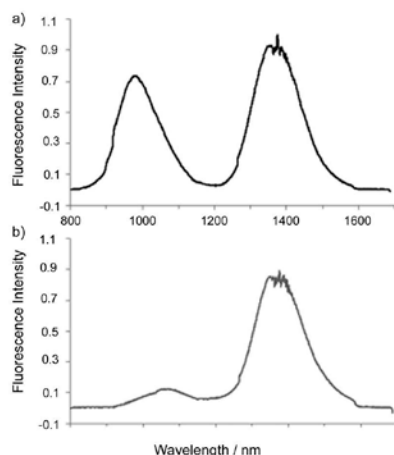


Figure 10. Fluorescence spectra of a mixture of 2.3 nm and 4.7 nm PbS nanoparticles in toluene (a) and in a solid film prepared by Sc-CO₂ deposition on glass (b).

is dissolved in toluene again. For the mixed PbS nanoparticle films prepared by solvent evaporation under ambient pressure, changes in the relative fluorescence peak intensity are observed but the values fluctuate depending on the locations of the film measured. Uniformity of nanoparticle films could be an important factor for studying optical properties of metal sulfide quantum dot films or fabricating reproducible devices.

3. Conclusion

PbS nanoparticles can be deposited uniformly on carbon-coated copper grids and on glass using Sc-CO₂ as a deposition medium. TEM images showed that PbS nanoparticles can form uniform 2D or 3D arrays in supercritical CO₂, while benchtop solution deposition usually displays non-uniform structures. SEM images also showed that PbS nanoparticles can penetrate into nanoscale holes in a Si substrate forming a close-packed array using the Sc-CO₂ process which cannot be achieved by a traditional solvent-deposition method. A specially designed apparatus for depositing PbS quantum dots on glass in Sc-CO₂ was described. The PbS nanoparticle films formed in Sc-CO₂ showed good areal coverage and uniformity, suitable for studying optical properties and energy-transfer phenomena between quantum dots in the near-infrared region. Further research along this direction is currently in progress.

Experimental Section

Chemicals and PbS Nanoparticle Synthesis

Hexanes, toluene, octadecene (ODE), bis(trimethylsilyl)sulfide (TMS), triethylphosphine (TOP), oleic acid (OA), ethanol, and methanol were purchased from Aldrich and used as received. Oleic acid-

capped PbS nanoparticles were synthesized in our lab using a literature procedure reported by Hines and Scholes.⁶⁶ The synthesized PbS nanoparticles were dispersed in toluene.

The size of PbS could be controlled by the ratio OA/ODE, injection and particle growth temperatures. For synthesizing small PbS nanoparticles, PbO (0.09 g), OA (0.25 mL), and ODE (3.75 mL) were added into a 3-neck reaction flask with vigorously stirring under a continuous flow of argon (Ar) gas at 150 °C for 1 h. Afterwards, 42 μ L TMS in 2 mL TOP was quickly injected into the system. The temperature was controlled around 70–90 °C and the reaction was carried out for another hour. For synthesizing large PbS nanoparticles, PbO (0.09 g), ODE (5 mL), TOP (2 mL) and OA (0.5 mL) were added into the reaction flask under Ar flow at 150 °C. A TMS (16 μ L) in TOP (1 mL) solution was then injected into the flask for the chemical reaction to take place. The particle growth temperature was controlled at 120–130 °C for 1 hr. More detailed information can be found in ref. [6].

Deposition of PbS Nanoparticles Using Sc-CO₂

The Sc-CO₂ deposition process was carried out using a 35.3 mL high-pressure stainless steel chamber. Carbon-coated copper grids or pieces of a Si wafer were immersed in a metal sulfide nanoparticle/toluene solution placed in a small vial. The chamber was charged with liquid CO₂ (60 atm) at room temperature over a period of 10 min and then the pressure was raised to 70 atm. The system was then heated to 40 °C to convert the liquid carbon dioxide to the supercritical fluid phase. At this time the pressure inside the chamber was about 145 atm. The ISCO pump then slowly raised the pressure up to 160 atm in the chamber. The high pressure apparatus was left at this condition (40 °C and 160 atm) for 30 min to reach an equilibrium state. The reason for increasing the pressure from 145 atm to 160 atm is to ensure the system pressure is consistent and reproducible. The PbS nanoparticles precipitated evenly and self-assembled to form a uniform 2D arrays on the TEM copper grid during the Sc-CO₂ phase. The method was reported previously for making gold nanoparticle arrays on Si surfaces.^[23,24,39] The particles are probably deposited by a gas-antisolvent (GAS) mechanism described previously in the literature,^[24,39] where an increasing amount of CO₂ alters the polarity of the toluene solvent rendering it unfavorable for particle stabilization in the colloid, which results in particle precipitation from solution.

The oleic acid-protected PbS nanoparticles can also form arrays on the TEM copper grids immersed in the toluene solution under atmospheric pressure. However, the benchtop solvent-evaporation process, due to high surface tension at the liquid/vapor interface, can lead to imperfect nanoparticle ordering forming isolated islands, percolating domains, locally high particle populations, and uneven surface coverage.^[30–32]

An apparatus for depositing PbS nanoparticles on a glass surface in Sc-CO₂ is shown in Figure 5. The device (Figure 5b) consists of two pieces of aluminum plates each with a circular opening in the center (0.5 inch diameter). A piece of glass is inserted between the two aluminum metal plates with two Teflon O-rings placed on each side of the flat substrate. The device can be tightened by turning the screws located in each corner of the metal plate. The O-rings placed on both sides of the flat substrate prevent leaking of nanoparticle solution. After loading a certain amount of the PbS nanoparticle solution, the device was placed in the Sc-CO₂ reactor (Figure 5a) at 40 °C and 160 atm for about 30 min. Because Sc-CO₂ has near zero surface tension, uniform nanoparticle films (Figure 5c) of different thickness can be formed using this device.

Instruments and Measurements

Carbon-coated copper grids purchased from Ted Pella were used to prepare samples for particle size determination from TEM images. The TEM samples were prepared by depositing a 4 μ L drop of the stabilized metal sulfide solution onto the grid or, if a higher density of nanoparticless was needed, by sequentially adding another drop after the first drop had dried. A Phillips CM 200 LaB₆ (Lanthanum Hexaboride Cathode) transmission electron microscope operating at 200 kV was used for both low and high resolution imaging. The average size of the PbS nanoparticles was obtained from the TEM images by measuring at least 300 particles using the ImageJ software. The electron diffractions of the metal sulfide particles were also measured by the Phillips CM 200 LaB₆ TEM. SEM images were collected with a Sirion instrument manufactured by FEI, Inc. The following parameters were used for the SEM field emission gun (FEG): an accelerating voltage of 10 kV, a spot size of 3, and a working distance of \sim 4.5 mm. Powder XRD patterns were recorded on a Bruker D8 Advance X-ray powder diffractometer with a graphite monochromatized CuK α (λ = 0.15406 nm) source. A scanning rate of 0.05° s⁻¹ was applied to record the pattern in the 2 θ range of 10–90°. UV/Vis near-infrared (NIR) spectra of PbS nanoparticles were obtained using a Cary 5000 Varian UV/Vis-NIR spectrophotometer scanning from 200 to 1800 nm. Fluorescence spectra were measured with a Horiba Jobin Yvon Nanolog 916B spectrometer equipped with an IGA 512 InGaAs near-IR detector.

Acknowledgements

The work at the University of Idaho was partially supported by DURI-AFRL (FA8650-06-D-5401). The work at the Air Force Research Laboratory (AFRL/RXPS) was supported by Dr. Kitt Reinhardt of AFOSR/RSE.

Keywords: energy transfer • fluorescence • nanoparticle films • supercritical fluids • PbS

- [1] J. Zhu, S. Liu, O. Palchik, Y. Koltypin, A. Gedanken, *J. Solid State Chem.* **2000**, *153*, 342.
- [2] F. E. Kruis, H. Fissan, B. Reilhinhauss, *Mater. Sci. Eng. B* **2000**, *69–70*, 329.
- [3] F. E. Kruis, H. Fissan, A. Peled, *J. Aerosol Sci.* **1998**, *29*, 511.
- [4] P. Wang, S. M. Zakeeruddin, J. F. Moser, M. K. Nazeeeruddin, T. Sekiguchi, M. Grätzel, *Nat. Mater.* **2003**, *2*, 402.
- [5] P. T. Guerreiro, S. Ten, N. F. Borrelli, J. Butty, G. E. Jabbour, N. Peyghambarian, *Appl. Phys. Lett.* **1997**, *71*, 1595.
- [6] M. A. Hines, G. D. Scholes, *Adv. Mater.* **2003**, *15*, 1844.
- [7] X. Zhao, I. Gorelikov, S. Musikhin, S. Cauchi, V. Sukhovatkin, E. H. Sargent, E. Kumacheva, *Langmuir* **2005**, *21*, 1086.
- [8] A. Kumar, A. Jakhmola, *J. Colloid Interface Sci.* **2006**, *297*, 607.
- [9] E. H. Sargent, *Adv. Mater.* **2005**, *17*, 515.
- [10] H. Hirata, K. Higashiyama, *Bull. Chem. Soc. Jpn.* **1971**, *44*, 2420.
- [11] P. K. Nair, O. Gomezdava, M. T. S. Nair, *Adv. Mater. Opt. Electron.* **1992**, *1*, 139.
- [12] T. Ding, R. Zhang, S. Long, J. J. Zhu, *Microelectron. Eng.* **2003**, *66*, 46.
- [13] F. Pang, X. Sun, H. Guo, J. Yan, J. Wang, X. Zeng, Z. Chen, T. Wang, *Opt. Express* **2010**, *18*, 14024.
- [14] V. Sukhovatkin, S. Musikhin, I. Gorelikov, S. Cauchi, L. Bakueva, E. Kumacheva, E. H. Sargent, *Opt. Lett.* **2005**, *30*, 171.
- [15] T. D. Krauss, F. W. Wise, D. B. Tanner, *Phys. Rev. Lett.* **1996**, *76*, 1376.
- [16] S. Zhou, Y. Feng, L. Zhang, *J. Mater. Res.* **2003**, *18*, 1188.
- [17] L. Bakueva, S. Musikhin, M. A. Hines, T. W. F. Chang, M. Tzolov, G. D. Scholes, E. H. Sargent, *Appl. Phys. Lett.* **2003**, *82*, 2895.
- [18] L. Cademartini, J. Bertolotti, R. Saplenza, D. S. Wiersma, G. von Freymann, G. A. Ozin, *J. Phys. Chem. B* **2006**, *110*, 671.
- [19] S. Wang, S. Yang, *Langmuir* **2000**, *16*, 389.
- [20] Y. Wang, N. Herron, *J. Phys. Chem.* **1987**, *91*, 257.
- [21] R. S. Kane, R. E. Cohen, R. Silbey, *Chem. Mater.* **1996**, *8*, 1919.
- [22] A. A. Clapp, I. L. Medintia, H. Mattoussi, *ChemPhysChem* **2006**, *7*, 47.
- [23] J. S. Wang, A. B. Smetana, J. J. Boeckl, G. J. Brown, C. M. Wai, *Langmuir* **2010**, *26*, 1117.
- [24] A. B. Smetana, J. S. Wang, J. J. Boeckl, G. J. Brown, C. M. Wai, *J. Phys. Chem. C* **2008**, *112*, 2294.
- [25] A. B. Smetana, J. S. Wang, J. J. Boeckl, G. J. Brown, C. M. Wai, *Langmuir* **2007**, *23*, 10429.
- [26] C. D. Bain, E. B. Troughton, Y. T. Tao, J. Evall, G. M. Whitesides, R. G. Nuzzo, *J. Am. Chem. Soc.* **1989**, *111*, 321.
- [27] L. Motte, F. Billoudet, M. P. Pileni, *J. Phys. Chem.* **1995**, *99*, 16425.
- [28] B. L. V. Prasad, S. I. Stoeva, C. M. Sorensen, K. J. Klabunde, *Langmuir* **2002**, *18*, 7515.
- [29] W. Du, X. Qian, X. Ma, Q. Gong, H. Gao, J. Yin, *Chem. Eur. J.* **2007**, *13*, 3241.
- [30] M. C. McLeod, C. L. Kitchens, C. B. Roberts, *Langmuir* **2005**, *21*, 2414.
- [31] X. M. Lin, H. M. Jaeger, C. M. Sorensen, K. J. Klabunde, *J. Phys. Chem. B* **2001**, *105*, 3353.
- [32] P. C. Ohara, W. M. Gelbart, *Langmuir* **1998**, *14*, 3418.
- [33] B. A. Korgel, D. Fitzmaurice, *Phys. Rev. Lett.* **1998**, *80*, 3531.
- [34] C. B. Murray, C. R. Kagan, M. G. Bawendi, *Annu. Rev. Mater. Sci.* **2000**, *30*, 545.
- [35] B. R. Hyun, A. C. Bartnik, L. F. Sun, T. Hanrath, F. W. Wise, *Nano Lett.* **2011**, *11*, 2126.
- [36] M. Achermann, M. A. Petruska, S. Kos, D. L. Smith, D. D. Koleske, V. I. Klimov, *Nature* **2004**, *429*, 642.
- [37] M. Achermann, M. A. Petruska, S. A. Crooker, V. I. Klimov, *J. Phys. Chem. B* **2003**, *107*, 13782.
- [38] S. W. Clark, J. M. Harbold, F. W. Wise, *J. Phys. Chem. C* **2007**, *111*, 7302.
- [39] J. Liu, M. Anand, C. B. Roberts, *Langmuir* **2006**, *22*, 3964.

Received: January 17, 2012

Revised: March 1, 2012

Published online on March 29, 2012

SECTION III

Mater. Res. Soc. Symp. Proc. Vol. 1409 © 2012 Materials Research Society
DOI: 10.1557/opl.2012.755

Lead Sulfide Quantum Dot Synthesis, Deposition, and Temperature Dependence Studies of the Stokes Shift

Joanna S. Wang, Bruno Ullrich, and Gail J. Brown

Air Force Research Laboratory, Materials & Manufacturing Directorate, Wright Patterson AFB,
OH 45433-7707, USA

ABSTRACT

We investigated the temperature dependence of the Stokes shift of PbS quantum dots (diameter 4.7 nm) deposited from solution on glass using a specially designed apparatus. By measuring the thermal alteration of the optical absorbance and photoluminescence in the range of 5 K – 300 K, we demonstrate that the Stokes shift shrinks from 135 meV at 5 K to 62 meV at 300 K. Extrapolation of the data presented predict an elimination temperature of the Stokes shift of about 460 K, corresponding to the thermal energy of the sum of prominent PbS phonon energies.

INTRODUCTION

Lead Sulfide quantum dots (QDs) have attracted considerable attention owing to the narrow direct band gap (0.41 eV) and large exciton Bohr radius, providing an excellent system for studying quantum confinement effects [1]. However, despite these extensive studies there are still opportunities to further understanding of the physics of the optical properties associated with the confined states. One such topic is the understanding of the origin of the Stokes shift between the peaks of photoluminescence (PL) and optical absorbance (OA) of PbS QDs. The PL of PbS QDs has been studied intensively during the previous years, where particular attention was paid to the thermal shift of the emission spectra [2-5]. In addition, some of the works compare both the room temperature absorption [3,5,6] and the absorption at cryogenic temperatures [5,7,8] with the PL spectra and show a redshift of the PL with respect to the absorption edge. This separation is referred to as the Stokes shift and is usually attributed to multi-phonon driven energy relaxations into the dark excitation state before luminescent transitions occur [9]. The influence of the size [7,9] and stoichiometry [9] on the Stokes shift was studied for PbS QDs but not its temperature dependence $S(T)$. The analysis of $S(T)$, which is of considerable importance for further understanding of the PL transition and the realization of technological applications including anti-Stokes cooling [10], is presented in this paper.

EXPERIMENTAL DETAILS

The PbS QDs used in this study were synthesized in organic solvents, with oleic acid as a capping agent, based on a method published in the literature [11]. The synthesis starts with the reaction of PbO with oleic acid to form lead oleate by heating oleic acid with PbO in a round bottom flask under Ar atmosphere while stirring. The temperature was kept at 150 °C for 1 hr. After this, a sulfide source, *bis*(trimethylsilyl) sulfide, was injected into the system and the reaction mixture was allowed to ripen for 1 hr at 100 °C. The PbS sample was then washed with

methanol, which removed the excesses of oleic acid and octadecene. The QDs were dried by a stream of N_2 and then dissolved in toluene. The size of the PbS QDs can be altered by changing the oleic acid/octadecene ratios and also can be controlled by changing injection and growth temperatures [11] during the synthesis.

Using this process, PbS QDs of different sizes have been selectively synthesized and deposited utilizing different deposition approaches in order to create thin films and close-packed arrays. For this study, PbS QDs with a diameter of ~ 4.7 nm were used, motivated by the room temperature emission wavelengths in the range $1.3\ \mu\text{m}$ - $1.55\ \mu\text{m}$, which is important for telecommunication applications. Indeed, the absorbance peak of the PbS solution used to form the films took place at around 1330 nm (0.932 eV) at 300 K.

The high-resolution transmission electron microscopy (HRTEM) image of the QDs is shown in Fig. 1 a and the powder x-ray diffraction (XRD) patterns of the dots - in comparison to the galena standard positions - are shown in Fig. 1 b. We chose to investigate the PL properties of the PbS QD film formed on glass employing solvent evaporation deposition to avoid any interference of the substrate with the optical properties. Employing the straightforward solvent evaporation deposition process, drying starts in the center causing the pale spot known as "coffee ring" (Fig. 1 c). The homemade apparatus for deposition consists of two aluminum plates, each with a circular 0.5-inch opening in the center (Fig. 1 d). A piece of glass is inserted between the plates with two Teflon o-rings placed on each side of the glass substrate in order to prevent leaking of the QD solution. The sample was formed by mixing $70\ \mu\text{L}$ of PbS QDs ($40\ \text{mg/mL}$, diameter 4.7 ± 0.5 nm) with $200\ \mu\text{L}$ toluene solvent. After keeping the PbS toluene solution in the dark for approximately 30 min at room temperature, the solvent was evaporated and the dry PbS/glass sample was removed from the holder.

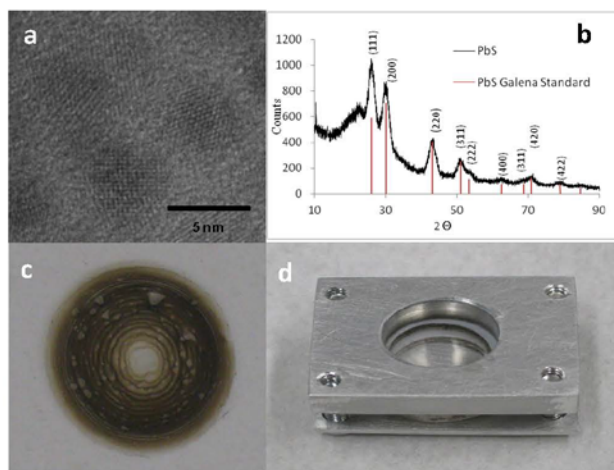


Figure 1. (a) HRTEM of PbS nanoparticles, (b) X-ray diffraction pattern of the PbS QDs, (c) the formed PbS QDs on glass (the diameter of PbS QD film is about 0.5 inch), and (d) the homemade solvent deposition apparatus.

The PL and OA measurements were carried out with two BOMEM Fourier transform spectrometers (standard and high-resolution). The PL was excited with the continuous wave (cw) 532 nm emission of a solid-state laser keeping the intensity at about 5 W/cm². The sample emission was detected with an InSb detector attached to the standard BOMEM and the sample temperature was controlled by an optical closed-cycle cryostat. The OA spectrum of the sample was determined via the transmittance, using the internal globar source of the high-resolution BOMEM in conjunction with the same InSb detector. The OA was calculated using $\log(I_0/I)$, where I_0 is the impinging light intensity and I is the transmitted light intensity. The sample temperature was again regulated with an optical closed-cycle cryostat.

DISCUSSION

Figure 2 shows the PL and OA spectra measured at 5 K for the thin-film of PbS QDs on glass. A clear Stokes shift of 135 meV is observed. This is comparable to the 150 meV Stokes shift at 10 K reported by Zhang and Jiang for 4.2 nm PbS QDs on sapphire [7]. At room temperature our measured Stokes shift was only 62 meV. In Figure 3 the measured PL and OA peak positions are plotted over the entire range from 5 K to 300 K. Clearly, the separation between the PL and OA peak positions decreases as the sample temperature is increased. In order to understand the origin of the temperature dependence of the Stokes shift, we first consider the temperature dependence of the OA and PL peaks separately.

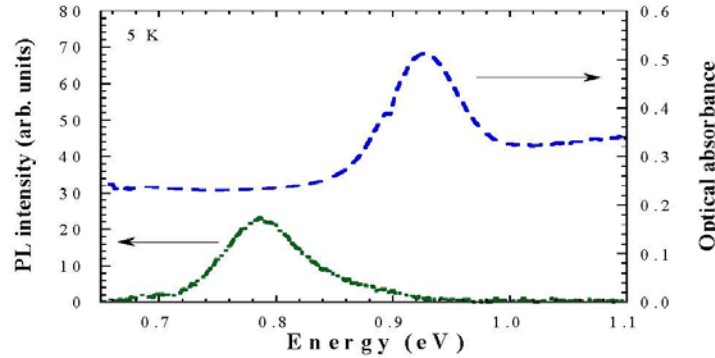


Figure 2. PL and OA spectra measured at 5 K.

Table I. Fitting parameters for the fits in Figure 3 done with Eq. (1)

Measurement	$E_g(0)$ (eV)	A (meV)	$\langle E_p \rangle$ (meV)
OA	0.922	23.4	15.5
PL	0.787	73.9	13.5

For the current work, the thermal band gap shift $E_g(T)$ is the key parameter. We use for this purpose the expression of Fan [12],

$$E_g(T) = E_g(0) + A / \{\exp(\langle E_p \rangle / kT) - 1\}, \quad (1)$$

where $E_g(0)$ is the low temperature limit of the band gap energy, A is the Fan parameter, which depends on the microscopic material properties, $\langle E_p \rangle$ is the average phonon energy responsible for the band gap variation, and kT is the thermal energy. The two sets of data were fit using Eq. (1) but required different fitting parameters. The fitting parameters are displayed in Table I. There is good agreement between the averaged $\langle E_p \rangle$ (≈ 14.5 meV) of these two fits and the value for bulk PbS (14 meV) [3,13]. However, the Fan parameter is much larger for the PL fit. This highlights a difference between the nature of the states involved in the PL and OA transitions.

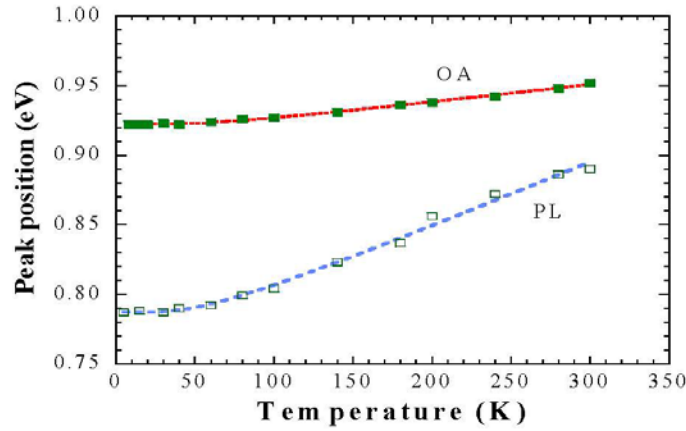


Figure 3. The symbols show the measured thermal shift of the PL (\square) and OA (\blacksquare) peaks. The dashed lines are the fits using Eq. (1).

For PbS QDs capped with oleic acid, the literature indicates that the PL involves a trap state, which is an acceptor state on the QD surface caused by unpassivated sulfur [14,15]. Hence, the difference between the OA and PL peak energies arises from the different processes involved in the two transitions: The OA process involves excitation from the hole confined state ($h1$) to the electron confined state ($e1$), while the PL process involves recombination of an excited electron with a lower energy hole, as illustrated in Fig. 4. If the holes were in the $h1$ state then the emitted photon energy would coincide with the absorption energy. For a Stokes shift to occur, the e-h recombination must take place at a lower energy state. For 1-2 nm PbS QDs, Fernée *et al.* reported that the trap state was at least 375 meV below the bulk PbS valence band edge [14]. The surface trap energy is known to vary with QD sizes [15]. For our 4.7 nm QDs the Stokes shift can be fit assuming hole trap states around 200 meV below the bulk valence band, as outlined in detail in Fig. 4. There are reports of very small Stokes shifts (~ 10 meV) at room temperature for well-passivated PbS, indicating that the surface states are an important factor in the measured Stokes shift [11,16].

In order to better visualize the temperature dependence of $S(T)$, the energy difference between the OA and PL peak energies is plotted versus T in Figure 5. Considering the good fit with Eq. (1) for the PL and OA data in Figure 3, the formula fitting $S(T)$ ought to be an expression like Eq. (1). We advocate the following expression for $S(T)$:

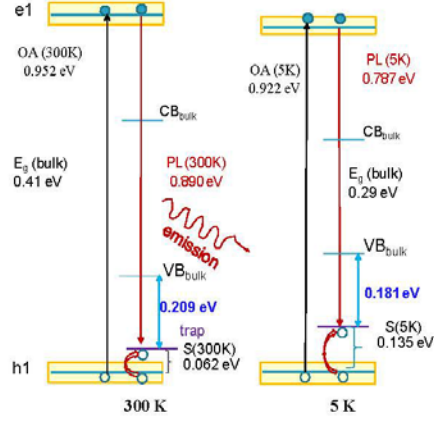


Figure 4. Schematic of the OA and PL transitions with hole trap states tied to the bulk PbS valence band edge. The shift of the trap state with temperature results in the temperature dependence of the Stokes shift.

$$S(T) = S(0) - C / \{\exp(\langle E_p \rangle / kT) - 1\}, \quad (2)$$

where, $S(0)$ is the Stokes shift at temperatures approaching 0 K, C is a constant, and $\langle E_p \rangle$ is again the average phonon energy.

The dotted line in Figure 5 shows the fit of the data with Eq. (2) using the fitting parameters of $S(0) = 0.135$ eV, $\langle E_p \rangle = 14.5$ meV and $C = 60.2$ meV. At low temperatures < 100 K, the dotted line matches the data better than at higher temperatures suggesting that at cryogenic temperatures the average phonon energy is responsible for the thermal variation of absorption and luminescent transitions. At higher temperatures, however, multi-phonon processes contribute to $S(T)$.

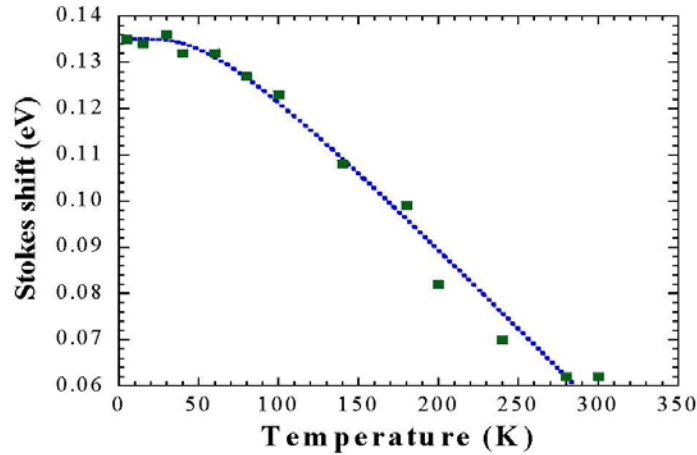


Figure 5. The difference between the energies of the OA and PL peaks in Figure 3. The dotted line is the fit using $\langle E_p \rangle = 14.5$ meV, $S(0) = 0.135$ eV, and $C = 60.2$ meV in Eq. (2).

Equation 2 allows the calculation of the critical temperature T_c where $S(T_c)=0$, i.e.,

$$T_c = \frac{\langle E_p \rangle}{k \ln \left(\frac{C}{S(0)} + 1 \right)}, \quad (3)$$

where $k=8.62 \times 10^{-5}$ eV/K, and we find that $T=457$ K, corresponding to $kT=39.4$ meV. It is evident that more work needs to be done in order to achieve a clear understanding of the reduction of the Stokes shift with increasing temperature, but we note that this number matches quite well the sum of $\langle E_p \rangle=14.5$ meV and the phonon energy $E_{LO}(\Gamma)=26$ meV [2]. We have just begun with the systematic analysis of PbS QDs prepared with different methods on various substrates and will carry out further experiments at elevated temperatures.

In conclusion, we studied the temperature dependence of the Stokes shift of PbS QDs. The thermally induced shifts of the OA and PL peaks were fit with the Fan equation. Similarly, the energy difference between these two peaks can be equivalently well fit with an equation of identical structure. At temperatures ≤ 100 K, $S(T)$ is related to the bulk average phonon energy (~ 14 meV), while a trap model was required to explain the observed values of $S(T)$. The data collected up to 300 K predict the existence of a critical temperature around 460 K, where no Stokes shift takes place, corresponding to the sum of two prominent phonon energies.

REFERENCES:

1. J. J. Peterson and T. D. Krauss, *Nano Lett.* **6**, 510 (2006).
2. L. Turyanska, A. Patanè, M. Henini, B. Hennequin and N. R. Thomas, *Appl. Phys. Lett.* **90**, 101913 (2007).
3. M. S. Gaponenko, A. A. Lutich, N. A. Tolstik, A. A. Onushchenko, A. M. Malyarevich, E. P. Petrov and K. V. Yumashev, *Phys. Rev. B* **82**, 125320 (2010).
4. B. Ullrich, X. Y. Xiao, and G. J. Brown, *J. Appl. Phys.* **108**, 013525 (2010).
5. B. Ullrich, J. S. Wang, and G. J. Brown, *Appl. Phys. Lett.* **99**, 081901 (2011).
6. C. Liu, K. Kwon, and J. Heo, *J. Non-Cryst. Solids* **355**, 1880 (2009).
7. J. Zhang, X. Jiang, *J. Phys. Chem. B* **112**, 9557 (2008).
8. J. Zhang and X. Jiang, *Appl. Phys. Lett.* **92**, 141108 (2008).
9. N. O. Dantas, P. M. N. de Paula, R. S. Silva, V. López-Richard, and G. E. Marques, *J. Appl. Phys.* **109**, 024308 (2011).
10. Y. P. Rakovich, J. F. Donegan, M. I. Vasilevskiy, and A. L. Rogach, *Phys. Stat. Sol. A* **206**, 2497 (2009).
11. M. A. Hines and G. D. Scholes, *Adv. Mater.* **15(21)**, 1844, (2003).
12. I. A. Vainshtein, A. F. Zatsepin, and V. S. Kortov, *Phys. Solid State* **41**, 907 (1999).
13. O. Madelung, *Semiconductors: Data Handbook*, 3rd ed. (Springer, Berlin, 2004).
14. M. J. Fernée, E. Thomsen, P. Jensen, and H. Rubinsztein-Dunlop, *Nanotech* **17**, 956 (2008).
15. A. Lobo, T. Muller, M. Nagel, H. Borchert, S.G. Hickey, and H. Weller, *J. Phys. Chem. C* **109**, 17422 (2005).
16. K. A. Abel, J. Shan, J.-C. Boyer, F. Harris, and F. C. J. M. van Veggel, *Chem. Mater.* **20**, 3794 (2008).

SECTION IV

Fourier spectroscopy on PbS quantum dots

Bruno Ullrich*, Joanna S. Wang, Xiaoyin Y. Xiao, Gail J. Brown
Air Force Research Laboratory, Materials & Manufacturing Directorate, Wright Patterson AFB, OH
USA 45433-7707

ABSTRACT

The manuscript summarizes our current research on PbS quantum dots. The emission and transmission features in the temperature range of 5 K - 300 K of 4.7 nm PbS quantum dots were investigated and theoretically analyzed with the Fan model, which is based upon the phonon-electron interaction. The model - although designed for bulk semiconductors - apply for quantum dots with the potential to determine fundamental properties such as the Debye temperature.

Keywords: PbS quantum dots, Fourier spectroscopy, photoluminescence, absorption, Fan model, Debye temperature

1. INTRODUCTION

The investigation of structures with dimensions in the nm regime, such PbS quantum dots (QDs), has been an active research topic since almost twenty years [1]. Much of the interest is based on possible optical device applications, which frequently require an intense photoluminescence (PL) output. Hence, the PL properties of PbS QDs caused an outburst of publications [2-11], while - among others - the specifics of the studies cover the PL efficiency [2], surface states [5], line width of the emission [6], temporally resolved PL [9], and the thermal dependence of the PL and transmittance (TR) spectra [11]. Based on our previous work [11], this paper summarizes and continues our theoretical analysis of the thermally induced band gap shift of colloidal PbS QDs deposited on glass. In particular, it is demonstrated that a model based on thermodynamics and a microscopic parameter, which includes basic material constants such as permittivity and effective carrier masses describes the thermal behavior extremely well. The work further enlightens the possibility to use the thermal band gap shift of QDs to determine the Debye temperature.

2. SAMPLE PREPARATION AND OPTICAL MEASUREMENTS

The sample was prepared in the following way: The QDs have been dissolved in toluene and capped with oleic acid and the solution was dispersed on glass using a specifically designed mount consisting of two aluminum plates separated by Teflon o-rings [11]. After 30 minutes at ambient conditions in the dark, the solvent evaporated and the coating became a solid colloid. The usual "ring-like" appearance of QD films prepared in this way indicates a variation of the film thickness, i.e., with increasing particle coverage towards the outside of the ring. The average size of the dots was determined to be 4.7 (± 0.5) nm.

For the optical measurements, BOMEM Fourier transform infrared (FTIR) spectrometers were employed. The technique differs considerably from the probably more common and known method incorporating monochromators; FTIR spectrometers consist basically of an interferometer (beamsplitter, a fixed mirror, and a moving mirror) including a reference laser and an attached detector. The capability of dynamic calibration mechanism during scanning due to the generated harmonic modulation of the reference laser beam, known as *Comes Advantage*, is the benefit of FTIR spectrometer with respect to dispersive instruments. Employing a BOMEM, the optical spectrum of the sample is not measured per se, i.e., the production of the result is done by mathematical means. By exciting the sample with a light source, an interferogram that has all the frequencies "encoded" is recorded, and, in order to obtain the actual emission or transmission spectrum, the signal is translated from the time domain, corresponding to the moving mirror position, to the frequency (energy) domain by Fourier transformation. The temperature dependence of the PL and TR was measured by mounting the samples in an optical cryostat hooked up to a temperature controller. Due to spectral range of concern (0.8 eV -1.0 eV), an InSb detector has been attached to the BOMEM. The optical excitation for the PL experiments was performed with a continuous wave (cw) solid-state laser emitting at 532 nm. The impinging laser intensity on the sample surface did not exceed 5 W/cm², while the TR data were collected by using the internal global source of the BOMEM spectrometer.

Quantum Dots and Nanostructures: Synthesis, Characterization, and Modeling IX,
edited by Kurt G. Eyink, Frank Szmulowicz, Diana L. Huffaker, Proc. of SPIE Vol. 8271,
82710A · © 2012 SPIE · CCC code: 0277-786X/12/\$18 · doi: 10.1117/12.905980

Proc. of SPIE Vol. 8271 82710A-1

3. EXPERIMENTAL AND THEORETICAL RESULTS

Besides the fairly long time PbS QDs have been in the focus of basic research, the PL properties reported in the literature were cumbersome regarding the comparability of the published results. Even more notable, no attempts have been addressed in order to explain the different PL results of PbS QD systems. For example, almost constant PL peak energies vs. temperature were reported [7], while in other papers a bulk-like behavior of the thermal PL peak shift was observed [9,10]. In context with the thermal influence on the emission properties, the question arose whether the common description, such as the well-known Varshni equation, which is frequently used for bulk semiconductors, applies for PbS QDs [9]. Detailed analysis of the subject revealed that it is indeed justified to describe the thermal band gap variation with a theory developed for bulk semiconductors - however, not necessarily with the Varshni relation. As early as 1951 [12], Fan derived a formula based on the electron-phonon coupling, which given by,

$$E_g(T) = E_g(0) + A / \{ \exp(\langle E_p \rangle / kT) - 1 \}, \quad (1)$$

where, $E(0)$ is the extrapolated PL peak (or TR minimum) energy at $T=0$ K, A is the Fan parameter, $\langle E_p \rangle$ is the average phonon energy, which is involved in the band gap alteration, and kT is the thermal energy reflecting the ambient temperature. Typically, PbS shows for lower temperatures (<50 -80 K) a nonlinear upturn, and at higher temperatures the peak shift reveals a linear dependence on the temperature. Figure 1 shows the thermal shift of the TR minimum and the PL peak for the sample. The symbols show the actual position and the dotted lines were calculated with Eq. (1). The fitting parameters are summarized in Table 1. The parameter Θ_D will be discussed later in the text. Figures 2 and 3 show corresponding spectra for selected temperatures.

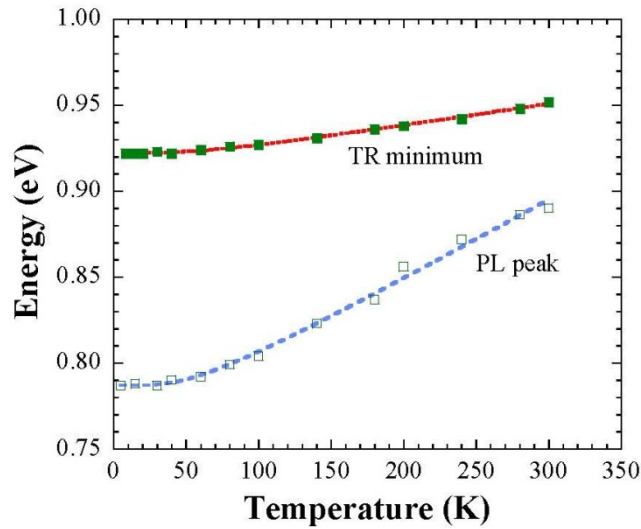


Figure 1. TR minima and PL peaks vs. temperature.

Table 1. Fit parameters used in Eq. (1).

Measurement	$E_g(0)$ (eV)	A (eV)	$\langle E_p \rangle$ (eV)	Θ_D (K)
TR	0.9223 ± 0.0003	0.0234 ± 0.0039	0.0155 ± 0.0019	180 ± 22
PL	0.787 ± 0.002	0.0720 ± 0.0168	0.0132 ± 0.0024	153 ± 28

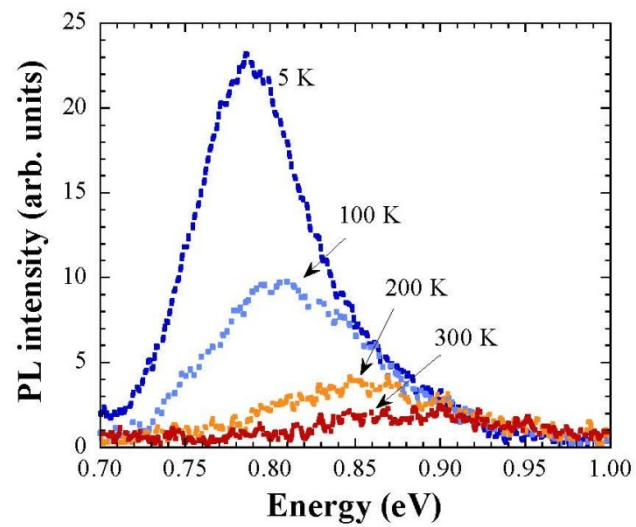


Figure 2. PL spectra at 5 K, 100 K, 200 K, and 300 K.

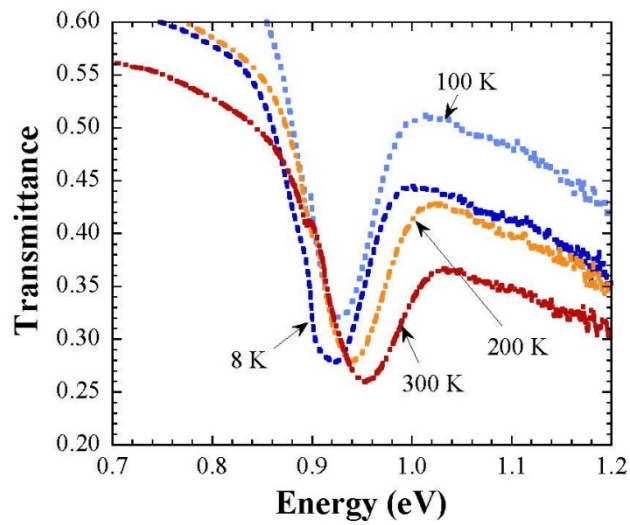


Figure 3. TR spectra at 8 K, 100 K, 200 K, and 300 K.

We found the answer to the discrepancies of the thermally induced PL peak shifts in the literature. PL experiments carried out specifically with lasers potentially “overexcite” the samples leading to extrinsic temperature dependences of the band gap. Reliable data are achieved by TR measurements performed with comparably low intensities, such as the emission of a globar. Laser excited PL data closer to the intrinsic material features (at least regarding the common shape of the thermal band gap dependence) can be collected by keeping the impinging laser power as low as possible, i.e., close to the PL threshold at 300 K - for the current sample it was about 5 W/cm².

We note that the Eq.(1) does not take into account the volume alteration with temperature. However, this effect is only 10-20% of the entire thermally induced band gap variation - and as pointed out by Vainshtein et al . [13] – for higher temperatures the Fan parameter A obtained by the fit considers both: The electron-phonon interaction and the thermal expansion. We further note that A itself is an energy, which is widely temperature invariant, expressed by [13,14],

$$A = \frac{e^2}{\sqrt{2}\hbar} (m_0 < E_p >)^{1/2} \frac{1}{4\pi\epsilon} \left(\frac{1}{\epsilon_\infty} - \frac{1}{\epsilon_0} \right) \left[\left(\frac{m_e}{m_0} \right)^{1/2} + \left(\frac{m_h}{m_0} \right)^{1/2} \right], \quad (2)$$

where, e ($=1.602 \times 10^{-19}$ As) is the elementary charge, \hbar ($=1.054 \times 10^{-34}$ Js) is Planck’s constant divided by 2π , m_0 ($=9.11 \times 10^{-31}$ kg) is the free electron mass, ϵ ($=8.854 \times 10^{-12}$ As/Vm) is the vacuum permittivity, ϵ_0 ($=150$) is the static and ϵ_∞ ($=16.8$) is the high frequency dielectric constant [11], and m_e ($=0.080$) and m_h ($=0.075$) is the effective electron and hole mass [11]. For the bulk PbS phonon energy ($=14$ meV) [9], Eq. (2) gives $A=0.0128$ eV, which is in acceptable agreement with the A value for the TR measurements (0.0234 eV) in table 1. Figure 4 visualizes Eq. (2) as a function of $<E_p>$. The A value of the PL data fit (0.0720 eV) is way off indicating that the PL analysis is less reliable than the conclusions based on TR data.

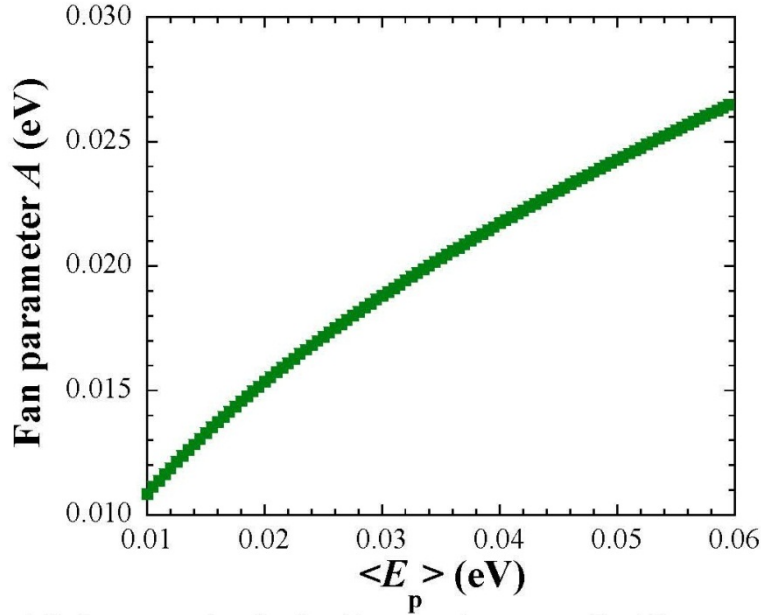


Figure 4. The Fan parameter A as a function of the average phonon energy $<E_p>$. A Fan parameter of 0.0720 eV (see PL fit in table 1) would require unrealistic large phonon energies.

We discuss now the fitting parameter Θ_b in table 1. The values were calculated with $\Theta_b = \langle E_p \rangle / k$, where k is the Boltzmann constant. It was pointed out in Ref. [11] that Θ_b corresponds to the Debye temperature showing fair agreement with the Θ_b data of bulk PbS. We further note that both measurements, TR and PL, by considering the error bars, delivered a common overlap pointing clearly to a value of around 180 K. That overlap of the fitting parameters was not achieved with the Varshni equation [11]. As a consequence, we conclude that fits with the empirical Varshni formula do not reveal the correct quantitative information about the QDs - the same conclusion was drawn for bulk semiconductors [13].

Specific attention deserves the ratio A/α where α is the temperature coefficient of the linear section in Fig. 1. Considering the TR data (from table 1, $A=0.0234$ eV, and $\alpha=1.3 \times 10^{-4}$ eV/K for $T \geq 140$ K [11]) the empirical formula,

$$\Theta_b = \langle E_p \rangle / k = A / \alpha \quad (3)$$

holds. Intuitively, Eq. (3) makes sense by calculating the constant Θ_b with the ratio of two constants, which are in relation to Θ_b . Nevertheless, more work is required to show whether Eq. (3) is a relation of generality but it seems that it applies for semiconductors, which possess a linear temperature dependence of the band gap above 200-250 K, as it is the case here and, for example, for GaAs [11].

4. CONCLUSIONS

FTIR spectroscopy on PbS QDs was performed in the temperature range of 5 K – 300 K. The Fan model, originally designed for bulk semiconductors, based on the phonon-electron interaction describes the results accurately. It appears that the model can be used for the determination of the Debye temperature for a specific “class” of semiconductors, which overcome the nonlinear thermal band gap dependence at fairly low temperatures (<250 K). The Fan model independence from the material dimensions is explained by the nature of the Fan parameter A , depending on microscopic parameters, which are widely unrelated to material dimensions and temperature variations. Further work is in progress to show the more general validity of the Fan model.

ACKNOWLEDGEMENT

This work was supported by the Air Force Office of Scientific Research (AFRL/RSE, Dr. Kitt Reinhardt).

REFERENCES

- [1] Borrelli, N. F. and Smith, D. W., “Quantum confinement of PbS microcrystals in glass,” *J. Non.-Cryst. Solids* 180, 25-31 (1994).
- [2] Fernée, M. J., Thomsen, E., Jensen, P. and Rubinsztein-Dunlop, H., “Highly efficient luminescence from a hybrid state found in strongly quantum confined PbS nanocrystals,” *Nanotech.* 17, 956-962 (2006)
- [3] Kim, D., Kuwabara, T. and Nakayama, M., “Photoluminescence properties related to localized states in colloidal PbS quantum dots,” *J. Lum.* 119-120, 214-218 (2006).
- [4] Peterson, J. J. and Krauss, T. D., “Fluorescence spectroscopy of single lead sulfide quantum dots,” *Nano Lett.* 6, 510-514 (2006).
- [5] Pendyala, N. B. and Rao, K. S. R. K., “Identification of surface states in PbS quantum dots by temperature dependent photoluminescence,” *J. Lum.* 128, 1826-1830 (2008).
- [6] Fernée, M. J., Jensen, P. and Rubinsztein-Dunlop, H., “Origin of the large homogeneous line width obtained from strongly quantum confined PbS nanocrystals at room temperature,” *J. Phys. Chem. C* 111, 4984-4989 (2007).
- [7] Lü, W., Yamada, F. and Kamiya, I., “Fabrication and coupling investigation of films of PbS quantum dots,” *J. Vac. Sci. Technol. B* 28, C5E8-C5E12 (2010).
- [8] Gaponenko, M. S., Yumashev, K. V. and Onushchenko, A. A., “Luminescence of lead sulfide nanocrystals in a silicate glass matrix,” *J. Appl. Spectroscopy* 77, 663-667 (2010).

- [9] Gaponenko, M. S., Lutich, A. A., Tolstik, N. A., Onushchenko, A. A., Malyarevich, A. M., Petrov, E. P. and Yumashev, K. V., "Temperature-dependent photoluminescence of PbS quantum dots in glass: Evidence of exciton state splitting and carrier trapping," *Phys. Rev. B* 82, 125320-1 - 125320-9 (2010).
- [10] Ullrich, B., Xiao, X. Y. and Brown, G. J., "Photoluminescence of PbS quantum dots on semi-insulating GaAs," *J. Appl. Phys.* 108, 013525-1 – 013525-5 (2010).
- [11] Ullrich, B., Wang, J. S. and Brown, G. J., "Analysis of thermal band gap variations of PbS quantum dots by Fourier transform transmission and emission spectroscopy," *Appl. Phys. Lett.* 99, 081901-1 – 081901-3 (2011).
- [12] Fan, H. Y., "Temperature dependence of the energy gap in semiconductors," *Phys. Rev.* 82, 900-905 (1951).
- [13] Vainshtein, I. A., Zatsepin, A. F. and Kortov, V. S., "Applicability of the empirical Varshni relation for the temperature dependence of the width of the band gap," *Phys. Solid State* 41, 905-908 (1999).
- [14] Fan, H. Y., "Photon-electron interaction, crystals without fields," Springer, Berlin, 157-233 (1967).

SECTION V

Mater. Res. Soc. Symp. Proc. Vol. 1449 © 2012 Materials Research Society
DOI: 10.1557/opl.2012.792

PbS Nanoparticles: Synthesis, Supercritical Fluid Deposition, and Optical Studies

Joanna S. Wang^a, Bruno Ullrich^{a,b}, and Gail J. Brown^a

^aAir Force Research Laboratory, Materials & Manufacturing Directorate, Wright Patterson AFB,
OH 45433-7707, USA

^bInstituto de Ciencias Físicas, Universidad Nacional Autónoma de México, Cuernavaca,
Morelos, México C.P. 62210

ABSTRACT

Lead sulfide (PbS) nanoparticles (NPs) of different sizes (2.0 nm - 14.4 nm) have been synthesized in our laboratory. By using those NPs, we formed colloidal films on glass and GaAs substrates employing a specialized supercritical fluid CO₂ (sc-CO₂) deposition method. The deposited films contain only the PbS NPs and the protecting group of oleic acids and require no polymer matrix. The NP films are solvent free, environmentally stable, and show good adhesion to the substrates. The sc-CO₂ deposition process can deposit films ranging in thickness from a few monolayers, in well ordered arrays, up to 0.5 μ m or greater. The photoluminescence (PL) properties of these nano-structured films were studied with Fourier transformation infrared spectroscopy from 5 K up to 300 K.

INTRODUCTION

The intrinsic features of PbS nanoparticles, particularly the clearly enhanced quantum confinement with respect to other attractive semiconductors such as CdTe and CdS, has boosted the research on PbS NPs during the past 15 years [1-5]. Particularly, the emission properties have attracted considerable attention [5-9]. While many of the PbS colloidal NPs studied have been embedded in glass or polymer matrices, we sought to develop a deposition process that could be compatible with standard semiconductor device processing, i.e. a cleaner process with less solvent residue and a process that enables close contact between the semiconductor surface and the NPs. We employed supercritical fluid CO₂ processes due to its near zero surface tension, the ability for the removal of solvents, and the capability to arrange NPs in ordered arrays [10-12] - a task difficult to achieve by traditional solvent deposition. To study the interactions of PbS NPs with semiconductor substrates colloidal PbS films of different NP diameters are highly useful. Glass substrates were used as control samples to isolate substrate charge transfer effects. For this study we developed both PbS NP synthesis and deposition processes using supercritical fluid CO₂. PbS nanoparticles precipitate evenly and self-assemble to form a uniform 2-D array on TEM copper grids, glass, and GaAs substrates during the sc-CO₂ deposition.

EXPERIMENTAL DETAILS

PbS QDs of different sizes have been selectively synthesized by the alteration of the following parameters: oleic acid/octadecene ratios, injection temperature, and growth temperature [13] during the synthesis. The TEM images of various PbS NPs synthesized with this process, ranging from 2.0 nm to 14.4 nm in diameter, are shown in Figure 1 below.

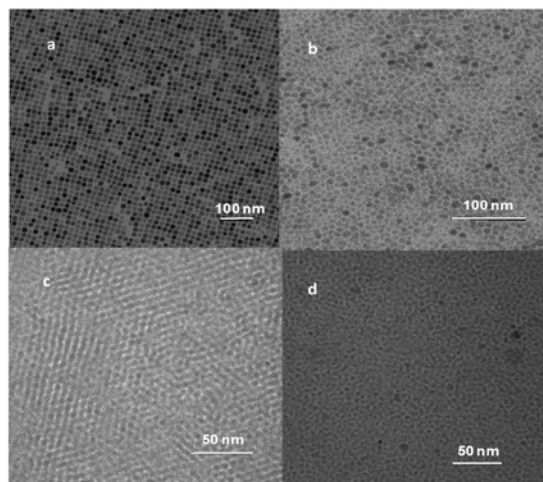


Figure 1. TEM images of PbS QDs with different sizes.
a: size = 14.4 ± 1.6 nm, b: size = 8.6 ± 1.1 nm,
c: size = 4.8 ± 0.54 nm, d: size = 2.8 ± 0.31 nm

Using the supercritical fluid CO₂ high pressure system (Fig. 2a) with our homemade sample deposition apparatus (Fig. 2b), we generated thin films and close-packed arrays. Samples were fabricated on a glass substrate to avoid any electronic charge transfer between the NPs and the inert insulating substrate. We developed a special process for creating uniform NP films over a 1 cm diameter area on glass slides using the apparatus in Fig. 2b.

The sample deposition apparatus consists of two aluminum plates, each with 2 circular 1 cm opening in the center. The specific design enables the production of two samples by deposition circle, which increased the coincident characterization activities and sample output. A piece of glass was inserted between the plates with two Teflon o-rings placed on each side of the glass substrate in order to prevent leaking of the QD solution. 40 μ L of PbS solution (depending on the thickness of PbS film required) at concentration of 10 μ g/ μ L were spiked into 200 μ L toluene solvent, followed by transferring the solution prepared into the sample holder in Fig. 2b. Using this adapted deposition device, the particular chemistry of the sc-CO₂ process was studied and optimized by feedback from the optical characterization.

The sc-CO₂ deposition process was carried out using a 35.3 mL high-pressure stainless steel chamber. The chamber was charged with liquid CO₂ (60 atm) at room temperature over a period of 10 min and then the pressure was raised to 80 atm. The system was then heated to 40 °C to convert the liquid carbon dioxide to the supercritical fluid phase. At this time the pressure inside the chamber was about 145 atm. The ISCO pump then slowly raised the pressure up to 180 atm in the chamber. The high pressure chamber was left at this condition (40 °C and 180 atm) for 30 min to ensure the system pressure is consistent and reproducible. In this process the PbS NPs are precipitated from the toluene solution by a gas-antisolvent (GAS) mechanism described previously in the literature [11,14], where an increasing amount of CO₂ alters the polarity of the toluene solvent and it becomes unfavorable for particle stabilization in the colloid, thus resulting

in the particles precipitation from solution. Not only are the NPs uniformly deposited on the substrate in a dense film, but also the toluene is completely removed by the sc-CO₂ cleaning process [14,15]. Fig. 2c shows a uniformly formed PbS sample with an areal density of 0.41 mg/cm² and a thickness of 0.854 μ m.

A different deposition process was required for the more fragile GaAs substrates. In this case, small pieces of heavily doped (5.2×10^{18} - 1.4×10^{19} cm⁻³) *p*-type GaAs:Zn (0.5×0.5 cm²) were immersed in a metal sulfide nanoparticle/toluene solution placed in a small vial. A schematic diagram of this process is shown in Fig. 2d. Similar sc-CO₂ process conditions as described above were used to precipitate the PbS nanoparticles evenly on the *p*-GaAs and remove the solvent from the vial. The resulting film on *p*-GaAs is shown as a SEM image in Fig. 2e. Unlike a benchtop solvent evaporation process, which has a high surface tension at the liquid/vapor interface and leads to imperfect nanoparticle ordering forming isolated islands, percolating domains, locally high particle population and uneven surface coverage [15-17], the sc-CO₂ process which has near zero surface tension leads to very uniform and densely packed films.

For the PL experiments, the sample was excited with the continuous wave (cw) emission at 532 nm of a solid state laser by keeping the impinging intensity below 50 W/cm². The PL emission was detected with a nitrogen cooled InGaAs detector attached to a BOMEM DA3 FTIR spectrometer. In order to measure the PL spectra at cryogenic temperatures, the sample was mounted in a closed cycle optical helium gas cryostat operating in the range 5 K- 300 K.

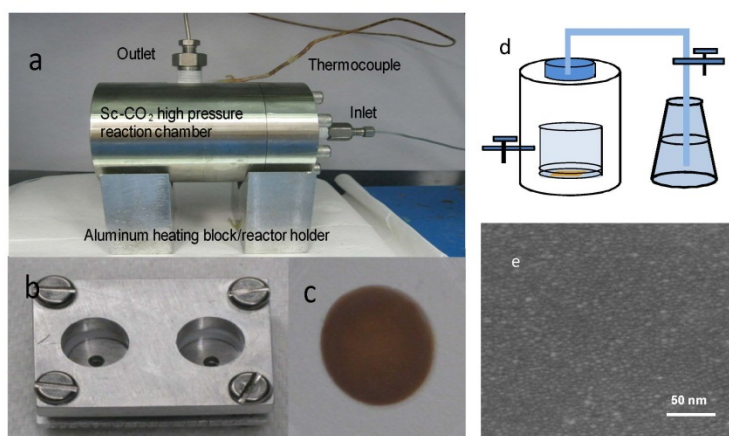


Figure 2. Deposition of PbS nanoparticles in supercritical fluid CO₂. (a) supercritical fluid CO₂ high pressure system, (b) home-made sampling apparatus and (c) deposited film using supercritical fluid CO₂. (d) schematic diagram of PbS deposition on GaAs substrate in sc-CO₂ and (e) SEM image of PbS on GaAs substrate using sc-CO₂ deposition method.

DISCUSSION

The traditional way to synthesize nanoparticles in our lab was using a water-in-oil based microemulsion method [10-12]. However, the microemulsion technique did not work for synthesis of PbS nanoparticles according to our experiments. The reason is likely due to the fact that the aqueous chemistry of lead ions is complicated and various lead species can exist in water depending on pH value and redox environment. It is difficult to control the dissolved lead ions in the aqueous solution to be in the pure Pb^{2+} state. Therefore, we chose to fabricate PbS nanoparticles by a traditional synthesis in organic solvents with oleic acid as a capping agent [13].

Figure 1 above shows TEM images of PbS with different sizes. PbS QDs synthesized as 14.4 nm are cubic lattice structures with tendency of self assembly showing a very ordered array (Fig. 1a). The 14.4 nm (Fig. 1a) and 8.6 nm (Fig. 1b) NPs have no absorbance features in near infrared region. The smaller PbS NPs, 4.8 nm (Fig. 1c) and 2.8 nm (Fig. 1d), show strong absorbance in UV-Vis-NIR region, and strong PL intensities with quantum confinement effects.

Optical microscope image results (Figures 3a, 3b, 3c and 3d) demonstrate the surface coverage features of the films on glass using both solvent and sc- CO_2 deposition methods. Apparently, the sc- CO_2 deposition method provides a more featureless surface with respect to the solvent deposition method. Optical images generated from sc- CO_2 (Figures 3b and 3d) demonstrate uniform and even coverage, whereas from solvent deposition method, coffee cup ring structures were shown in both Figures 3a and 3c.

Our XRD spectra indicate the PbS films have extended stability and PbS XRD pattern of PbS nanoparticles agrees very well with the standard reference data (JCPDS) for PbS galena structure, after nearly 2 year period of shelf life time. The film thickness was measured with DekTak 6 M Stylus Profiler instrument. 3000 μm scan length was used for a standard scan. The average scanned height corresponds to the PbS film thickness, for instance, the film thickness in Figure 2c, is 0.854 μm . The films on the glass deposited by sc- CO_2 are reasonably adhered to the glass surface and are not readily removed by an adhesive tape.

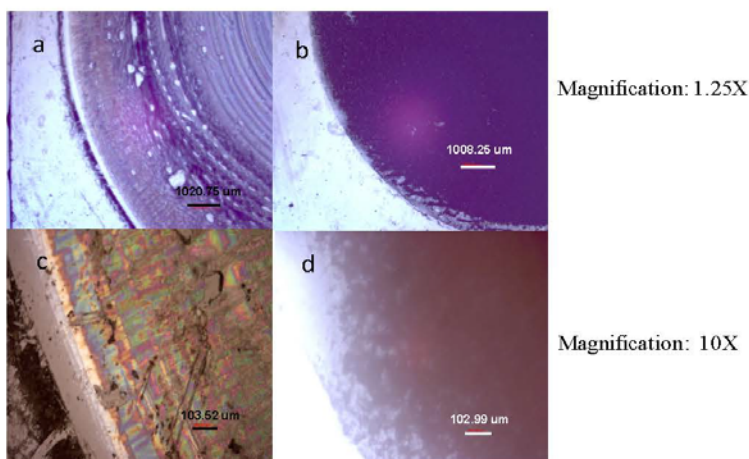


Figure 3. Microscope images of PbS films deposited on glass substrates. (a) solvent deposition and (b) sc- CO_2 deposition at magnification of 1.25X. (c) solvent deposition and (d) sc- CO_2 deposition at magnification of 10X.

For the PL study, PbS quantum dots (QDs) with diameters of 4.7 nm and 2.0 nm were used, motivated by the room temperature emission wavelengths in the range 1.0 μm -1.55 μm , which is important for telecommunication applications. Indeed, the absorbance peak of the PbS solution of 4.7 nm QDs used to form the films took place at around 1330 nm (0.932 eV) at 300 K. The optical properties of the PbS nanoparticle (4.7 nm diameter) films were measured by PL spectroscopy. The samples fabricated by the sc-CO₂ deposition process showed clearly detectable room temperature emission at 0.84 eV (1470 nm), which is blue-shifted from the bulk value at 0.41 eV due to quantum confinement effect. The PL wavelength of PbS QDs in solid films, versus in solution, show a red shift with increasing concentrations.

Figure 4 shows the emission of the PbS/*p*-GaAs sample at 5 K and 300 K. The spectra show the pronounced PbS QD emission and the photoluminescence of the *p*-GaAs at a low temperature (5 K). The intensity of PL emission at 5 K is about 3 times higher than that at room temperature (300 K). PbS films on glass and a GaAs substrate, formed by the sc-CO₂ deposition method, show a strong photoluminescence intensity attributed to the narrow particle size distribution and homogenous particle morphology, while PbS films deposited by traditional solvent deposition method have weak signal intensities attributed to particle non-uniformity.

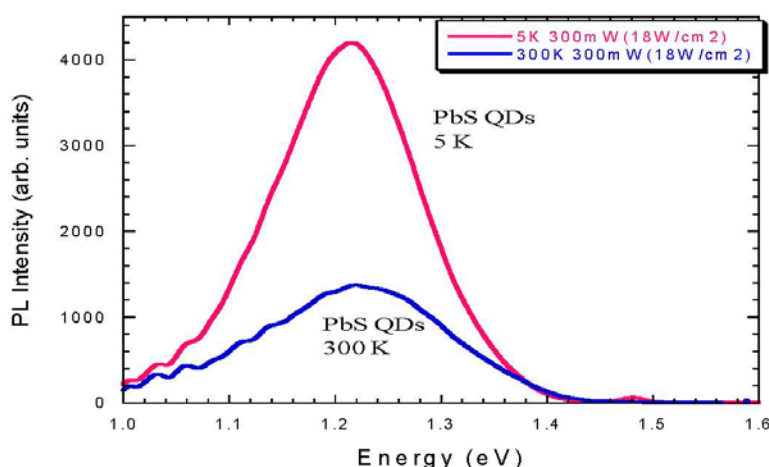


Figure 4. PL of the PbS/*p*-GaAs sample at 5 K and 300 K excited with a laser intensity of 18 W/cm². The emission of the GaAs substrate was observed in addition to the PL of the QDs.

CONCLUSION

PbS QDs in different sizes were synthesized in our laboratory. An apparatus for depositing PbS QDs on glass substrates employing a sc-CO₂ solution deposition method is described. The PbS QDs deposited in this way have shown improved uniformity and a good coverage in

comparison with conventional solution deposition. PL emission of the PbS/p-GaAs sample at 5 K and 300 K were measured in this study. The spectra show the pronounced PbS QD emission at a low temperature (5 K). The intensity of PL emission at 5 K is about 3 times higher than that at room temperature (300 K). PbS films on glass and GaAs substrate formed by the sc-CO₂ deposition method show strong PL intensity attributed to the narrow particle size distribution and homogenous particle morphology. An important future application of PbS quantum dots will be the formation of optoelectronic hybrid devices. Prospective partner for these hybrids are the III-V compound GaAs and related semiconductors, which are the current main players in the field of optoelectronic devices.

REFERENCES

1. L. Bakueva, S. Musikhin, M. A. Hines, T. W. F. Chang, M. Tzolov, G. D. Scholes and E. H. Sargent, *Appl. Phys. Lett.* **82**(17), 2895 (2003).
2. J. J. Peterson and T. D. Krauss, *Nano Lett.* **6**(3), 510 (2006).
3. A. Osherov, J. P. Makai, J. Balazs, Z. J. Horvath, N. Gutman, A. Sa'sr and Y. Golan, *J. Phys.: Condens. Matter* **22**, 262002, (2010).
4. R. D. Schaller, J. M. Pietryga, S. V. Goupalov, M. A. Petruska, S. A. Ivanov and V. Klimov, *Phys. Rev. Lett.* **95**, 196401 (2005).
5. R. Dalven, *Infrared Phys.* **9**, 141, 1969.
6. V. Biju, R. Kanemoto, Y. Matsumoto, S. Ishii, S. Nakanishi, T. Itoh, Y. Baba and M. Ishikawa, *J. Phys. Chem. C* **222**, 7924, (2007).
7. T. Y. Liu, M. Li, J. Ouyang, M. B. Zaman, R. Wang, X. Wu, C. S. Yeh, Q. Lin, B. Yang and Kui Yu, *J. Phys. Chem. C* **113**, 2301, (2009).
8. K. A. Abel, J. Shan, J. C. Boyer, F. Harris and F. C. J. M. Veggel, *Chem. Mater.* **20**, 3794 (2008).
9. T. Zhang, H. Zhao, D. Riabinina, M. Chaker and D. Ma, *J. Phys. Chem. C* **114**, 10153, (2010).
10. J. S. Wang, A.B. Smetana, J. J. Boeckl, G. J. Brown and M. Wai, *Langmuir* **26**(2), 1117 (2010).
11. A. B. Smetana, J. S. Wang, J. J. Boeckl, G.J. Brown and C. M. Wai, *J. Phys. Chem. C* **112**, 2294 (2008).
12. A. B. Smetana, J. S. Wang, J. J. Boeckl, G. J. Brown, C. M. Wai, *Langmuir* **23**, 10429 (2007).
13. M. A. Hines, and G.D. Scholes, *Adv. Mater.* **15**, 1844 (2003).
14. J. Liu, M. Anand and C. B. Roberts, *Langmuir* **22**, 3964 (2006).
15. M. C. McLeod, C. L. Kitchens, C. B. Roberts, *Langmuir* , **21**, 2414, (2005).
16. X. M. Lin, H. M. Jaeger, C. M. Sorensen and K.J. Klabunde, *J. Phys. Chem. B* **105**, 3353 (2001).
17. P. C. Ohara, and W. M. Gelbart, *Langmuir* **14**, 3418 (1998).

SECTION VI

Emission of Precipitation Deposited PbS Quantum Dots on Polyethylene Terephthalate

Bruno Ullrich^{*}, Andrew R. Markelonis, Joanna S. Wang, and Gail J. Brown

Air Force Research Laboratory, Materials & Manufacturing Directorate, Wright Patterson AFB,
OH 45433-7707, USA

ABSTRACT

Centrifuge enforced precipitation was used to disperse PbS quantum dots (diameter 4.7 nm) on polyethylene terephthalate. By employing double frequency Fourier transform spectroscopy, we studied the emission properties of the sample. Gaussian shaped emission spectra from cryogenic temperatures up to room temperatures were observed, demonstrating the potential of PbS quantum dots to be used as light emitters in combination with organic matrices. One interesting feature is that the linewidth of the emission spectrum does not follow the expected thermal broadening.

INTRODUCTION

Starting in the 1970s, composites of various inorganic semiconductors, which fulfill certain required technological functionalities, have been developed, further matured, and successively employed in mass-market electronic and optoelectronic devices [1,2]. These heterogeneous materials revolutionized nearly all areas of life. More recently, cost effective chemically tailored hybrids, i.e., the combination of organic and inorganic semiconductors – attributed as a *marriage of convenience* - attracted growing research interest about ten years ago [3,4]. Boosted by the envisaged technological impact of hybrid nanoscience, the research focused on the chemical bonding essentials of inorganic (metals and semiconductors) quantum dots (QDs) on polymeric surfaces and the embedding in polymer matrices [5,6]. The production of polymer-inorganic nanocomposites (PINCs) is equally motivated by economical and technological reasons [7], i.e., the fairly low production costs of polymers, their intrinsic capability of “free-shaping” combined with their low-weight and elasticity are an extremely attractive host for inorganic additives in the form of QDs. Various methods are used to produce PINCs: synthetic techniques, physical methods, electrochemical formation, chemical vapor deposition, and electrophoretic deposition [7-9]. Given that photoluminescence (PL) is the prerequisite for light emitting device structures, the PL properties of various QDs, such as CdS, CdTe [10,11], and PbS [12-14], have been intensively studied. The clearly enhanced quantum confinement with respect to most III-V and II-VI compound semiconductors [15], explains the explicit interest in QDs of the IV-VI semiconductor PbS. In this article, we present our first attempt to form light emitting colloidal PbS QD films on polyethylene terephthalate (PET).

EXPERIMENTAL DETAILS

A commercial solution of 4.7 nm PbS QDs in toluene with oleic acid as ligands was used to fabricate the sample, i.e., 12.5 μ L of the PbS QDs in a toluene solution (40 mg/mL) with oleic acid as capping reagents were added to 5 mL ethanol in an 8 mL sample vial with the PET substrate on the bottom. The deposition of the particles from the solution was enforced by using

precipitation in a centrifuge deposition method (CDM) for 8 min at 3200 rpm. Afterwards, by removing the solution and drying the sample in air, the QD film was obtained (Fig.1a). Thus, in contrast to previous works, which embedded the QDs in polymers or used PET as a carrier for Fano filters containing PbS QDs [5,6,10,16], we straightforwardly created a QD film on PET hybrid material. A transmission electron microscope (TEM) image of colloidal PbS QDs, deposited under the identical conditions as for the PET substrate but on a copper TEM grid, is shown in Fig. 1b. The TEM image reveals the random nature of the QD deposition, but overall shows a fairly continuous film. Because the deposition process is due to centrifugal force, there is no mechanism for the QDs to rearrange into close-packed, uniform layers and leads to partial clustering. Overall, at optical microscope resolutions, the QD film appears uniform with good coverage of the (4.5 mm by 4.5 mm) PET surface.

We do not know the bonding specifics between the QDs and the PET but QDs can bind to polymeric surfaces through van der Waals forces [17], hydrogen-bonding [5], electrostatic linkage [18], and covalent bonding [7]. Furthermore, ligand stabilized QDs are able to bond to specific sites on monomers [19]. To test for weak binding processes, like van der Waals and electrostatic linkage, we attempted to remove the QDs from the PET through several processes. The QD films did not peel off during bending, and light mechanical abrasion. For instance, the PbS QD film did not come off with a scotch tape test or when rubbed with a cotton tip, indicating that the PbS QD film on PET was robust enough for potential device applications. One advantage of this relatively simple deposition process is that it creates a durable QD film on a flexible substrate in which the QDs are readily available on the PET surface for further functionalization or interaction with external media. In addition, the QD film had measurable light emission at 1348 nm at room temperature which shows promise for future optical devices. The emission properties of the QD/PET hybrid are our primary interest.

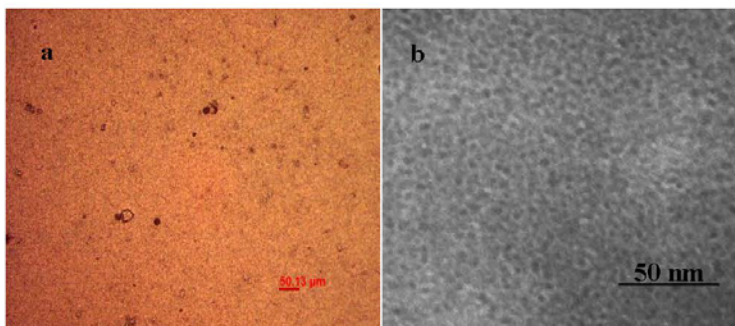


Figure 1. (a) Optical microscope image of PbS QD film on PET (10X magnification), (b) TEM image of PbS QDs on a TEM copper grid, both samples fabricated using CDM.

DISCUSSION

For the PL experiments, the optical excitation of about 30 W/cm² was provided by the 532 nm continuous wave (cw) emission of a solid-state laser. The PL was measured by a double modulation Fourier transform infrared spectroscopy (FTIR) technique [20]. The double modulation technique was necessary due to the rather weak PL of the sample at room

temperature. The luminescence was measured using a nitrogen cooled InGaAs detector and a quartz beamsplitter in the Bomem DA3 FTIR. The luminescence was measured from 5 K up to 300 K using a closed-cycle refrigeration cryostat with a diamond window.

Figure 2 shows the PL spectra measured at 5 K and 300 K. The broken line represents the measured PL intensity I as a function of the emitted photon energy $h\nu$ and the solid line the fit using the Gaussian intensity distribution,

$$I(h\nu) = A \times \exp(-(h\nu - h\nu_p)^2 / (2w^2)), \quad (1)$$

where A is the peak height, $h\nu_p$ is the center energy of the PL peak, and w defines the peak width parameter, which is related to the full-width at half maximum (FWHM) by $\text{FWHM} = 2.35 \times w$. While the PL emission is weaker at 300 K, as expected, the decrease is less than an order of magnitude, which is quite good. The same QD starting solution when dried on a glass substrate showed a much larger peak shift (100 meV) and intensity drop with temperature [21]. The 40 meV PL peak shift from 5 K to 300 K in the QD/PET sample is comparable to the 30 meV shift in the QD/glass absorption peak.

There are a few notable differences for the CDM deposited PbS QDs on PET and other QD films formed by a supercritical CO_2 fluid process or solution deposition on GaAs and glass, respectively. [13,14] For instance, the temperature dependent shift of the PL peak energy is linear (see Fig. 3) versus following the expected Fan equation [14] behavior, especially at low temperatures (< 50 K) where there should be very little change in the emission line energy. This linear behavior is related to alterations of the electronic state of the QDs caused by the laser irradiance [14]. We also noticed that the data are more scattered in Fig. 3 than other fits we have reported. Hence, it is possible that colloidal PbS QDs on PET substrates are subject to photo-induced changes under laser irradiation more than PbS QDs on inert substrates such as glass,

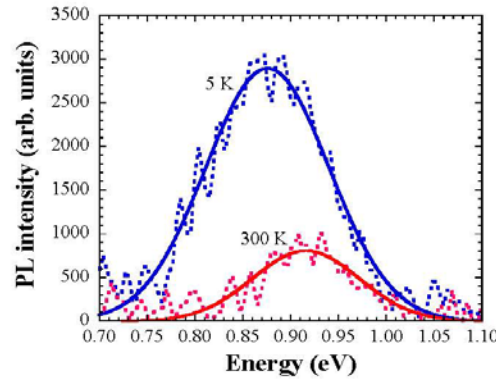


Figure 2. PL spectra at 5 K and 300 K. The broken line was measured and the solid lines represent the fits using Eq. (1).

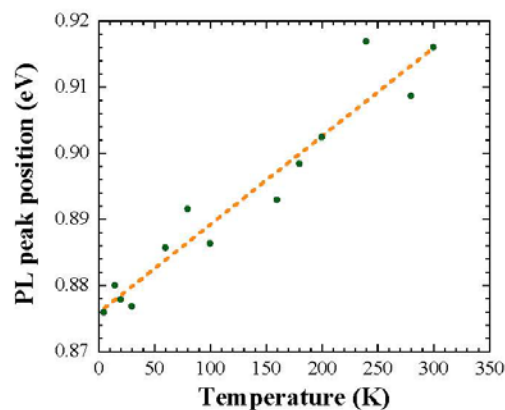


Figure 3. Peak energy position vs. temperature evaluated with the Gaussian fits using Eq. 1.

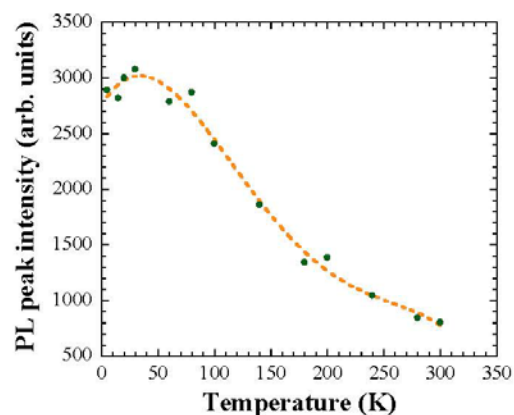


Figure 4. PL peak intensity (parameter A in Eq. 1) vs. temperature evaluated from the Gaussian fits.

altering the established bonding linkages at the PET surface build-up during deposition. It seems that the organic substrate plays an active part in the thermal properties of the PL spectra of PbS QDs. On the other hand, the PL peak intensity vs. temperature in Fig. 4 is very similar to the result reported for PbS QDs on glass [22].

Another notable difference for the CDM deposited PbS QDs on PET versus other QD films we previously studied is the PL peak FWHM is actually narrower at 300 K than at 5 K. The

result is unusual because it differs considerably from the previously reported thermally induced FWHM broadening, which was described by the Bose distribution function of longitudinal optical (LO) phonons [13,22,23]. The FWHM does broaden from 5 K to 150 K (see Fig. 5) but then begins to narrow for $T > 200$ K. There are very few mechanisms that could potentially explain a narrowing of the PL FWHM and capable of negating thermal broadening. The question is what recombination mechanism dominates at higher temperatures that is not a factor below 200 K? One example where the PbS QD environment caused a reduction in the PL FWHM is found in the work of Lin *et al.* [24], who investigated the PL of PbS QDs in different solutions including methanol, which is chemically related to PET. The quantum yield of PbS QDs in methanol is as low as 9 %, while a quantum yield of 82 % is achieved with PbS QDs in toluene, and by lowering the polarity of the hosting solution, the FWHM of the PL shrinks [24]. In our case, other than the duration of laser irradiation, only the sample temperature was changed - so to have a similar change in the QD environment, an alteration in the charge surrounding of the QD is required. This effect might occur if there is a change in the charge trapping at the QD surface above 150 K. However, other possible temperature dependent mechanisms need to be considered. Exploring the cause of the emission line width narrowing is left to further studies.

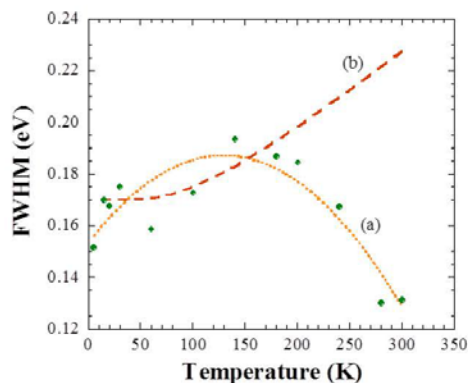


Figure 5. FWHM dependence of the PL spectra vs. temperature: The symbols along curve (a) represent the FWHM determined from the PL fits using Eq. (1). The guide for the eyes, the dotted line, is a polynomial fit. The broken line (b) shows the calculated expected behavior based on the Bose distribution function of longitudinal optical phonons [13,22].

CONCLUSIONS

In conclusion, we have demonstrated that the merger of PbS QDs with an organic substrate results in a light emitting surface structure, demonstrating the possible technological application potential of PINCs at ambient conditions. The centrifuge deposition process used in the sample fabrication is very straightforward and creates a durable QD film on PET substrates. The CDM process is amenable to deposition on a wide variety of substrates. We have used this process to deposit PbS QDs on paper, metal foil, glass and GaAs substrates. The photoluminescence results promote further research on these hybrids in order to optimize the emission features through

improvements of the colloid deposition process, and to understand the mechanisms, which cause the uncommon temperature dependence of the PL line width.

This work was supported by the Air Force Office of Scientific Research (AFRL/RSE, Dr. Kitt Reinhardt).

*Also with Instituto de Ciencias Físicas, Universidad Nacional Autónoma de México, Cuernavaca, Morelos, México C.P. 62210.

REFERENCES

1. S. O. Kasap, *Principles of Electronic Materials and Devices*, 2nd Edition (McGraw Hill, New York, 2002).
2. M. Grundmann, *The Physics of Semiconductors* (Springer, Berlin, 2006).
3. R. Schroeder and B. Ullrich, *Appl. Phys. Lett.* **81**, 556 (2002).
4. E. Gerstner, *Nature: Materials Science and Nanotechnology - News & Features*, July 2002.
5. W. H. Binder, C. Kluger, M. Josipovic, C. J. Straif, G. Friedbacher, *Macromolecules* **39**, 8092 (2006).
6. W. H. Binder, M. Lomoschitz, R. Sachsenhofer, G. Friedbacher, *J. Nanomaterials*, Article ID 613813, (2009).
7. S. Li, M. M. Lin, M. S. Toprak, D. K. Kim, M. Muhammed, *Nano Reviews* **1**, 5214 (2010).
8. S. Guenes, K. P. Fritz, H. Neugebauer, N. S. Sariciftci, S. Kumar, and G. D. Scholes, *Solar Energy Materials & Solar Cells* **91**, 420 (2007).
9. J. Akhtar, M. Afzaal, M. A. Vincent, N. A. Burton, I. A. Hillier, and P. O'Brien, *Chem. Comm.* **47**, (2011).
10. H. Du, G. Q. Xu, W. S. Chin, L. Huang, W. Ji, *Chem. Mater.* **14**, 4473 (2002).
11. I. Gorelikov and E. Kumacheva, *Chem. Mater.* **16**, 4122 (2004).
12. W. Lü, F. Yamada, and I. Kamiya, *J. Vac. Sci. Technol. B* **28**, C5E8 (2010).
13. B. Ullrich, X. Y. Xiao, and G. J. Brown, *J. Appl. Phys.* **108**, 013525 (2010).
14. B. Ullrich, J. S. Wang, and G. J. Brown, *Appl. Phys. Lett.* **99**, 081901 (2011).
15. F. W. Wise, *Acc. Chem. Res.* **33**, 773 (2000).
16. L. Chen, H. Yang, Z. Qiang, H. Pang, L. Sun, Z. Ma, R. Pate, A. Stiff-Roberts, S. Gao, J. Xu, G. J. Brown, and W. Zhou, *Appl. Phys. Lett.* **96**, 083111 (2010).
17. Y. Min, M. Akbulut, K. Kristiansen, Y. Golan, J. Israelachvili, *Nature Materials* **7**, 527 (2008).
18. S. Kinge, M. Crego-Calama, D. N. Reinhoudt, *ChemPhysChem* **9**, 20 (2008).
19. A. Haryono, W. H. Binder, *Small* **2**, 600 (2006).
20. B. Ullrich and G. J. Brown, *Rev. Sci. Instrum.* **83**, 016105 (2012).
21. B. Ullrich, J. Wang, X. Xiao, G. Brown, *Spectroscopy Photonics International Engineering (SPIE)*, **8271**, 82710A-1 (2012).
22. L. Turyanska, A. Patané, M. Henini, B. Hennequin, and N. R. Thomas, *Appl. Phys. Lett.* **90**, 101913 (2007).
23. M. S. Gaponenko, A. A. Lutich, N. A. Tolstik, A. A. Onushchenko, A. M. Malyarevich, E. P. Petrov, and K. V. Yumashev, *Phys. Rev. B* **82**, 125320 (2010).
24. W. Lin, K. Fritz, G. Guerin, G. R. Bardajee, S. Hinds, V. Sukhovatkin, E. H. Sargent, G. D. Scholes, and M. A. Winnik, *Langmuir* **24**, 8215 (2008).

Stability Studies of Lead Sulfide Colloidal Quantum Dot Films on Glass and GaAs Substrates

Joanna S. Wang*, Elizabeth H. Steenberg, Howard E. Smith,
Lawrence Grazulis, Jeremy A. Massengale, Bruno Ullrich, and Gail J. Brown,
Air Force Research Laboratory, Materials & Manufacturing Directorate, Wright Patterson AFB,
OH 45433-7707, USA

ABSTRACT

The stability of colloidal PbS quantum dot (QD) films deposited on various substrates including glass and GaAs was studied. Over a period of months, the QD film sample was re-tested after being left unprotected in air under ambient conditions. Despite exposure to 532 nm laser excitation and cooling to cryogenic temperatures, the initial photoluminescence (PL) remained stable between tests. We also retested a set of samples that had remained under ambient conditions for over 2 years. To track potential changes to the QDs over time, X-ray photoelectron spectroscopy (XPS), transmission electron microscopy (TEM), powder X-ray diffraction (XRD), optical microscopy, UV-Vis-NIR spectrophotometry and atomic force microscopy (AFM) were employed. Evidence points towards oxidation enforced shrinking of the active QD volume causing a blue shift of the absorption and photoluminescence. The presented studies are important for reliability expectations of light emitters based on PbS QDs.

Keywords: PbS quantum dots, photoluminescence, deposition, supercritical CO₂, UV-Vis-NIR spectrophotometry, X-ray photoelectron spectroscopy, X-ray diffraction, atomic force microscopy.

1. INTRODUCTION

Thin films of semiconductor quantum dots (QDs) are emerging as an important class of materials for electronic and optoelectronic devices such as field-effect transistors [1-3], photodetectors [4-7], light-emitting diodes [8-10], metamaterials [11-13], and solar cells [14,15]. As a consequence, the optical and electrical stability of colloidal quantum dots, such as PbS, used in devices is an important issue. For example, the effects of photo-oxidation exposure on the surface state of colloidal PbS QD films have drawn attention during the last decade [16-20]. Detrimental impacts to the morphology and optical properties of PbS QD films can occur via processes such as oxidation, heating or UV induced degradation. The oxidation-induced reduction in the size of the PbS “core” increases quantum confinement, causing shifts of the PL peak and the absorption onset to higher energies. To date, most investigations of IV-VI QDs’ stability have focused on thermally activated oxidation of PbX QD solutions or solid films, which rapidly decreased the physical and electronic size of the QDs, increasing the confined state energy separation and causing excitonic blueshifts of absorption and emission spectra [16-18]. However, the rate of aging of PbS QDs in ambient environments has not been thoroughly studied.

In this study, the stability of the PbS QD films, under ambient conditions was tested, with particular attention to any changes in the oxidation state of the QDs over a period of several months. Two sets of PbS QD films were fabricated, one set on glass and the other on 1 cm by 1 cm pieces of semi-insulating GaAs. The impact of the PbS QD film deposition processes on QD stability was also studied in these two sets. The aging of these films was investigated using photoluminescence (PL), UV-Vis-NIR spectrophotometry, X-ray photoelectron spectroscopy (XPS), transmission electron microscopy (TEM), powder X-ray diffraction (XRD), and atomic force microscopy (AFM). Fundamental investigations are required to systematically measure the rate of any degradation in the films due to short term exposure to ambient conditions during material and device fabrication processes, and to explore the need for device encapsulation over the long term. As reported in the literature [18], QD oxidation causes a considerable blue shift of both the absorption and the luminescent transitions. Therefore, the optical properties are an accurate means for tracking changes in the QD oxidation.

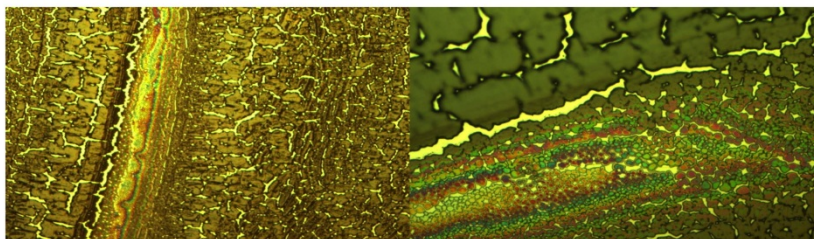
Quantum Dots and Nanostructures: Synthesis, Characterization, and Modeling X, edited by Kurt G. Eyink,
Diana L. Huffaker, Frank Szmulowicz, Proc. of SPIE Vol. 8634, 86340T · © 2013 SPIE
CCC code: 0277-786X/13/\$18 · doi: 10.1117/12.2002499

Proc. of SPIE Vol. 8634 86340T-1

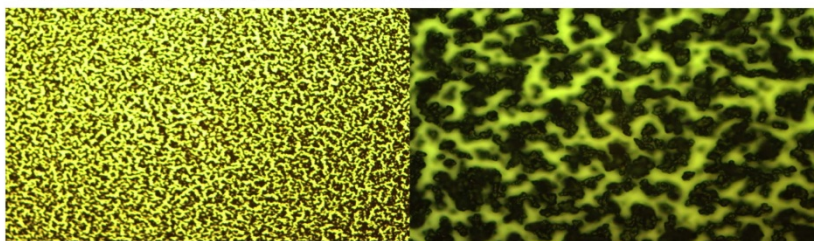
2. SAMPLE PREPARATION AND OPTICAL MEASUREMENTS

The films were formed employing supercritical fluid CO₂ deposition (SFD) and solvent deposition (SDM) methods. Oleic acid-capped PbS nanoparticles were synthesized in our lab using a procedure reported by Hines and Scholes [21]. The synthesized PbS QDs were dispersed in toluene. The SFD process was carried out using a 35.3 mL high-pressure stainless steel chamber. For both the glass slide and GaAs substrates the QD solution was contained on top of the substrate for the solvent removal by the SFD process. For the glass substrates a special apparatus was designed to cover larger diameters uniformly but the GaAs substrate was too fragile for this apparatus so smaller (1 cm by 1 cm) squares of GaAs were placed in a small vial with the PbS QD solution and then placed in the CO₂ high pressure chamber. Presumably, the supercritical fluid CO₂ deposition is governed by a gas-antisolvent (GAS) mechanism described previously in the literature [22-24], where an increasing amount of CO₂ alters the polarity of the toluene solvent and becomes unfavorable for particle stabilization in the colloid, thus resulting in the particles precipitating from solution. The PbS QDs precipitate evenly and self-assemble in a uniform array on the substrates during SFD. The method was reported previously for making Au, Ag₂S and CdS nanoparticle arrays on Si surfaces [22-24]. The oleic acid protected PbS QDs can also form films on the substrates immersed in the toluene solution under atmospheric pressure. This procedure is referred to as SDM. However, the benchtop solvent evaporation process, due to high surface tension at the liquid/vapor interface, can lead to imperfect nanoparticle ordering, forming isolated islands, percolating domains, locally high particle populations, and uneven surface coverage [25-27].

The optical images of PbS QDs on GaAs and glass fabricated by the SFD and SDM methods were taken by using Axiotron II Inspection Microscope. The solution deposition method using *p*-GaAs substrates resulted in coffee rings, long range channels and fractures in both 10 and 50 fold magnifications. However, SFD samples revealed a uniform material coverage over the entire substrate area, with some fractures. These fractures probably are due to the dryness via solvent removal in the sample deposition process. The initial optical images were taken immediately after the deposition process. For example, Fig. 1 shows the initial images of SDM and SFD films on semi-insulating (S.I.) GaAs. Despite the colors seen in the images below, the PbS QD films appear gray to the naked eye. Based upon the images taken at both 10 and 50 fold magnifications, the microscope images from initial and final measurements months later closely resemble each other. This gives an indication that the structural stability of the PbS QD films is quite reliable.



PbS QDs deposited on S.I. GaAs using SDM (07.25.12); optical microscope measurements were taken on 07.31.2012, (left) 10X and (right) 50X magnifications.



PbS QDs deposited on S.I. GaAs using SFD (07.31.12); optical microscope measurements were taken on 07.31.2012 (left) 10X and (right) 50X magnifications.

Figure 1. Optical microscope images of (top) PbS (SDM) on S.I. GaAs substrate and (bottom) PbS (SFD) on S.I. GaAs substrate.

3. RESULTS AND DISCUSSION

3.1 Absorption studies of PbS films deposited by SDM and SFD

The UV-Vis-NIR spectra of PbS QDs were obtained using a Cary 5000 Varian UV-Vis-NIR spectrophotometer scanning from 400 to 1600 nm. In this study the absorbance of SFD PbS QDs on a glass substrate was measured. The sample remained unprotected under the ambient conditions for 4.3 months, and the absorbance was measured again. About a 20 nm (15 meV) blue-shift was observed from the initial 1304 nm peak wavelength to the final 1284 nm peak wavelength. The peak shift is presumably caused by an oxidizing effect due to the exposure to air. The oxidation of Pb and S on the outer surface of the QDs reduces the active size and thereby creates a blue-shift [18], as shown in Fig. 2 (top). In the same manner the PbS QD film deposited on glass by SDM was measured. The fabricated sample was stored at ambient conditions and was measured again ~4.6 months later. During this period of time the maximum peak wavelength blue-shifted 34 nm (25 meV) from 1304 nm initially to 1270 nm as shown in Fig. 2 (bottom). The absorbance of the films made by the SFD method shifted less than SDM films because the SDM deposited films possess a relative larger surface area due to the uneven, porous, and “coffee ring” changes in density, which presents favorable conditions for oxidation. On the other hand, the films deposited by SFD possess a compact and uniform coverage, which is less influenced by air.

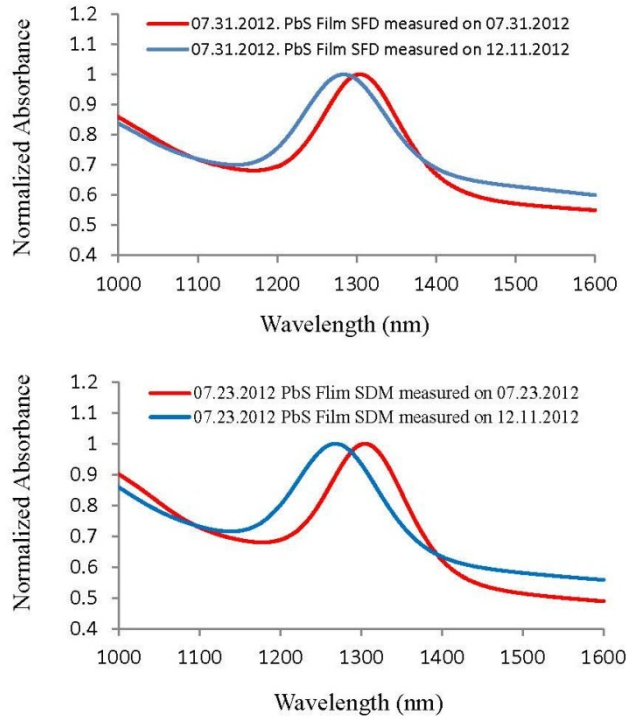


Figure 2. (Top) Absorbance spectra of PbS QDs on glass using SFD. The duration between 2 measurements is 4.3 months; (Bottom) Absorbance spectra of PbS QDs on glass using SDM. The duration between 2 measurements is 4.6 months.

3.2 Photoluminescence study of PbS QD films over three months

Room-temperature photoluminescence (PL) of the four samples was measured approximately once a month for three consecutive months, with the first of these measurements made approximately two months after QD deposition and storage in air. The samples were measured in a cryostat with a CsI window and optically pumped with a frequency-doubled Nd:YAG laser (532 nm) at an intensity of 0.76 W/cm^2 . A Bomem DA3 FTIR spectrometer was used to collect the PL spectra. Each spectrum was fit with a Gaussian curve to determine the peak position and FWHM, and the data are shown in Table 1.

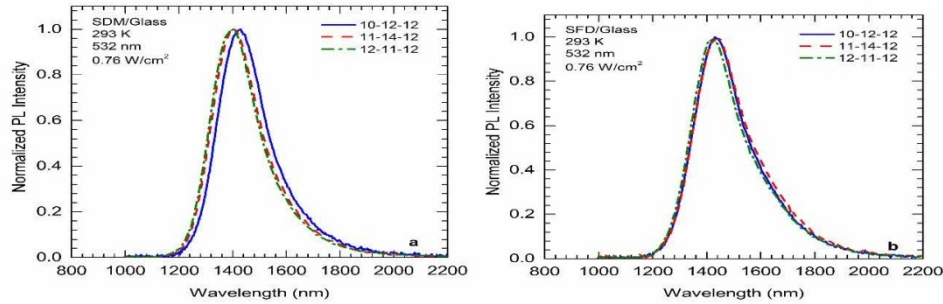


Figure 3. Room temperature PL measurements over three months on samples a) SDM and b) SFD deposited on glass.

Figure 3 displays the normalized PL spectra for the SDM (Fig. 3a) and SFD (Fig. 3b) samples on glass. From the first month to the second month, a blue shift in the PL peak position of 21 nm (13 meV) for the SDM sample was observed while the FWHM increased by 2 meV. The second to the third month shows no change in the FWHM and a smaller change in the peak blue shift, only 8 nm (5 meV). The SFD sample on glass first experiences a small red shift in the PL peak position, 5 nm (3 meV), from the first to the second month and then a subsequent 13 nm (8 meV) blue shift from the second to the third month. The FWHM varied by 4 meV over the three months. These shifts in the peak position for the SFD sample are within the experimental error of $\pm 5 \text{ meV}$, so effectively this sample showed no change in the PL spectra over the three months.

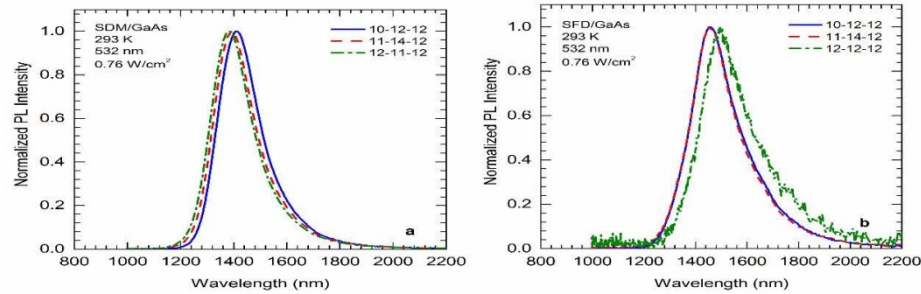


Figure 4. Room temperature PL measurements over three months on samples a) SDM and b) SFD deposited on GaAs.

The normalized spectra for the samples deposited on GaAs are shown in Fig. 4: SDM (Fig. 4a) and SFD (Fig. 4b). The PL peak position for the SDM sample blue shifts by 16 nm (10 meV) and 11 nm (7 meV) from the first to the second and the second to the third months, respectively. The FWHM is the smallest for this sample and varies by 5 meV over the three months. The SFD sample peak position and FWHM remain essentially constant from the first to the second month, varying only by 3 nm (2 meV), but a substantial red shift of 48 nm (27 meV) is

observed in the third month along with a large decrease in the intensity resulting in more noise on the spectrum. The red shift and intensity decrease are drastic and unexpected; however, this was the only sample that was thermally cycled to 4 K for temperature-dependent PL measurements.

The SFD samples experienced less change in the PL peak position over the first two months compared to the SDM samples, 5 nm (3 meV) and 3 nm (2 meV) versus 21 nm (13 meV) and 16 nm (10 meV), respectively. From the second to the third month, the peak position of the SDM samples shifted by half the amount from the first to the second month, while the peak shift of the SFD samples increased. The change in the FWHM of all the samples was less than 5 meV over the three months. Overall, the PL of the SFD samples was more stable than that of the SDM samples.

Table 1. Summary of Gaussian fit parameters to the PL spectra.

Method	Substrate	Sample	Peak Position (nm, meV)	FWHM (meV)
SDM	Glass	7/23/2012		
		10-12-12	1432, 866	141
		11-14-12	1411, 879	143
		12-11-12	1403, 884	143
SFD	Glass	7/31/2012		
		10-12-12	1445, 858	152
		11-14-12	1450, 855	156
		12-11-12	1437, 863	153
SDM	GaAs	7/25/2012		
		10-12-12	1417, 875	123
		11-14-12	1401, 885	126
		12-11-12	1390, 892	128
SFD	GaAs	7/31/2012		
		10-12-12	1469, 844	143
		11-14-12	1466, 846	141
		12-12-12	1514, 819	146

3.3 X-ray photoelectron spectroscopy (XPS)

XPS was used to assess the chemical stability of PbS QDs deposited on glass substrates by both the SFD and SDM methods. The Pb 2f, S 2s and O 1s transitions were examined for evidence of chemical shift [28, 29]. The spectra were acquired on a Perkin-Elmer Phi 5100 system, equipped with a non-monochromatic magnesium X-ray source and a hemispherical energy analyzer. Data manipulation and quantification were performed using CasaXPS software [30], applying published atomic sensitivity factors [31]. Chemical state determination was performed by fitting the spectra with component peaks of mixed Gaussian/Lorentzian (G/L) character. The proper mixture was determined for each spectrum individually, by determining the best statistical fit to its C 1s peak. The mixture value varied from G55/L45 to G30/L70, presumably due to differences in emission-induced surface charge. The fitting was done after subtracting the photoelectron signal contribution due to excitation by Mg X-ray source satellites, and after performing Shirley (P 4f, O 1s) or linear (S 2s) background subtraction.

Figure 5 shows the XPS measurements obtained approximately 2 months and 6 months after initial deposition (top and bottom halves of the figure, respectively) from both the SFD and SDM depositions (left and right halves, respectively). Each half of the figure is divided into two pairs of Pb 4f and S 2s photoelectron transitions. The raw XPS data are represented with red lines. Each of these transitions is broken into its chemical components of PbS and PbSO_x. Note that each Pb 4f photoelectron has two major peaks corresponding to 5/2 and 7/2 spin-orbit coupling. The time elapsed since deposition is shown inset in each graph in days (d). At approximately two months, for both depositions, the S 2s and Pb 4f spectra show substantial amounts of two different oxidation states (curves a, c, e and g). The chemical shift is considerably larger for the S 2s transition than for the Pb 4f transition, but in both cases the

observed shift is consistent with the formation of PbSO_3 and PbSO_4 [31,32]. That said, the Pb 4f chemical shifts of the various Pb_xO_y compounds are difficult to distinguish from PbS and PbSO_4 compounds [28,31]. However, the O 1s transition (not shown) is able to distinguish the presence of Pb_xO_y compounds, and it does not show evidence of Pb_xO_y . Therefore, the two main chemical components observed in both the Pb 4f and S 2s spectra correspond to PbS and PbSO_x .

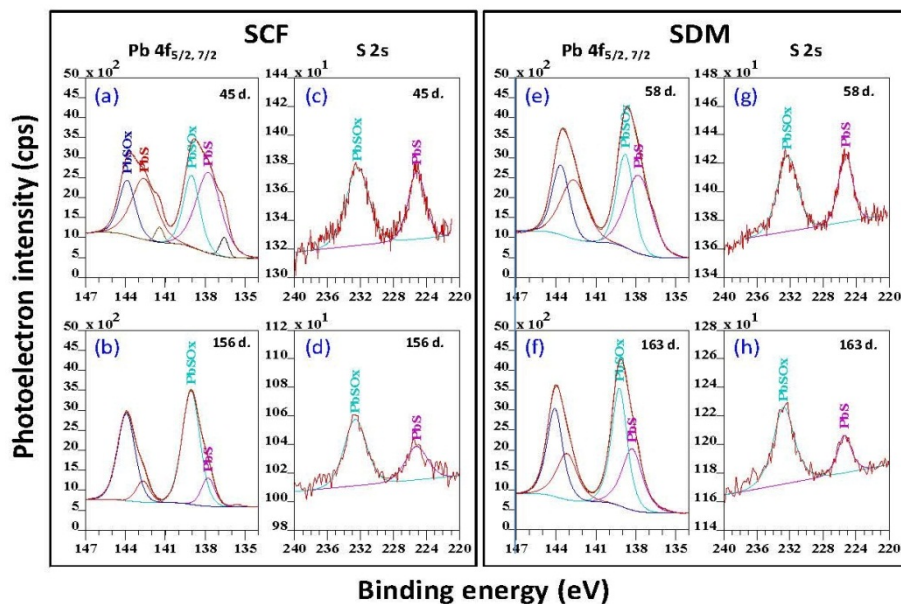


Figure 5. Pb 4f and S 2s photoelectron transitions obtained from the SFD and SDM of PbS QD films on glass with chemical states fitted.

In the spectra acquired ~6 months after deposition (bottom half of the figure), all samples have undergone substantial additional oxidation: the proportion attributed to PbSO_x has grown and the proportion of PbS has diminished. The changes are qualitatively similar in both the S 2s and Pb 4f spectra. The S 2s spectra reveal that the oxidation is occurring at the sulfur atom site. And while lead spectra show additional oxidation that could be consistent with the formation of either PbSO_x or Pb_xO_y , the O 1s spectra again establish no evidence for Pb_xO_y formation.

3.4 X-ray diffraction (XRD) studies of PbS films deposited by SDM and SFD

The X-ray diffraction (XRD) is a rapid analytical technique primarily used for phase identification of a crystalline material and can provide information on unit lattice dimensions. Powder X-ray diffraction (XRD) patterns were recorded on a Bruker D&Advance X-ray powder diffractometer with graphite monochromatized Cu $K\alpha$ ($\lambda = 0.15406$ nm) source. A scanning rate of $0.05^\circ \text{ s}^{-1}$ was applied to record the pattern in the 2θ range of 10 – 90° . The crystal structure of PbS is the galena structure and its XRD peak positions are well established.

According to our XRD measurement, the 4.7 nm sized PbS QDs possess the galena structure as expected. Before we discuss the deposited films stability, it is necessary to understand the nature of the QD aging process and the stability of PbS QDs in solution. We monitored the degradation of the PbS QDs (4.7 nm) stored in solution over 3 years. During this period the PbS solution was stored at 4°C in the dark. The XRD diffraction peaks remained unchanged during the first year. After the 2nd year the PbS QDs in solution gradually decayed and the diffraction peaks slowly diminished except for the 220 peak which was enlarged significantly comparing with the initial

measurement. This indicates that the PbS QD solution shelf life after synthesis is about one year. More important, however, is the long term stability of the prepared films.

The initial XRD measurement of a PbS QD film (4.7 nm) deposited by the SDM method on glass in 2009 is shown in Figure 6 (top). This sample was then left under ambient conditions for an extended period of time. After two and a half years the PbS film was remeasured by XRD (Figure 6 bottom). Overall there is not much phase transformation suggesting the PbS QD film is quite stable when exposed to air under the normal ambient conditions.

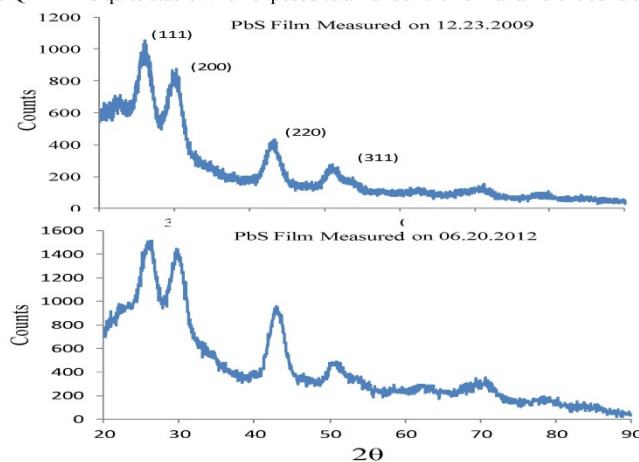


Figure 6. XRD measurements of a PbS film (4.7 nm) on glass measured in 2009 (top) and 2012 (bottom) which were prepared by SDM.

3.5 Atomic force microscope (AFM) studies of PbS films deposited by SDM and SFD

AFM was used to characterize the general morphology of the PbS QD films deposited by SFD and SDM on both glass and GaAs. Both preparation methods produced similar morphologies when viewed at the micrometer size scale (see Figure 7a, which shows 10 μm x 10 μm AFM image). Clearly, two types of features are generally observed, i.e. “plateaus” of densely packed QDs and deep cracks. The “plateaus” are 100 nm to 300 nm thick relative to the substrate and the cracks are 1 μm or less wide. Since the films are not continuous as deposited by either method, a second deposition would be required to fill in these small cracks in order to use the films in electrical devices. The SFD method is well suited for depositing nanoparticles into < 1 μm dimensions [22]. Figure 7b is a 3D representation of the same data shown in Figure 7a.

Although the fissures might appear to extend to the substrate, higher magnification images from these areas revealed that this was not the case. Instead, QDs are always distributed along the bottom surfaces of these fissures, with an average thickness of 20 to 50 nm, as determined by measuring the height of the QDs relative to scratches made

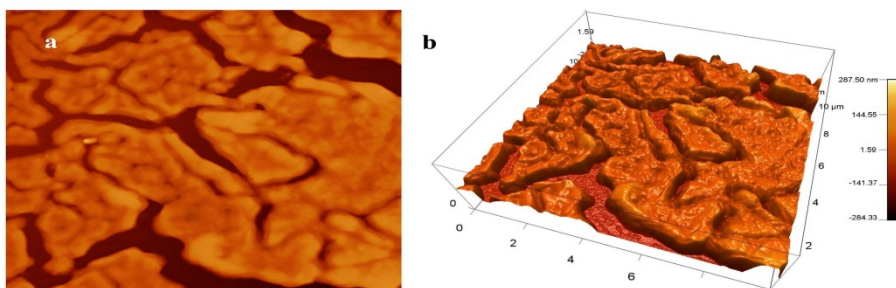


Figure 7. (a) 10 μm x 10 μm image of the general surface morphology; (b) 3D representation of figure 7a

through the QD layer to the substrate. That is, the minimum value of the height scale of Figure 7b represents the top of the QD layers within the fissures, some 20 to 50 nm above the substrate surface.

3.6 Transmission electron microscope (TEM) studies of PbS films deposited by SDM and SFD

For this part of the aging study we monitored PbS colloidal QDs deposited on carbon coated copper grids over approximately 2.6 years using SDM and SFD methods. Figure 8 shows the TEM profile of these PbS QDs formed by SDM and SFD. Here, TEM measurements taken on 04/13/10 (initial), on 11/03/11 (1.6 years), and 12/11/12 (2.6 years) are compared. We observed clearly that the QDs aged in air lose their faceting and are more diffuse in shape and size. The active average QD diameter appears to reduce as described in the literature [18]. The shapes of QDs become more irregular, and the size distribution considerably broadens when samples were stored under the ambient

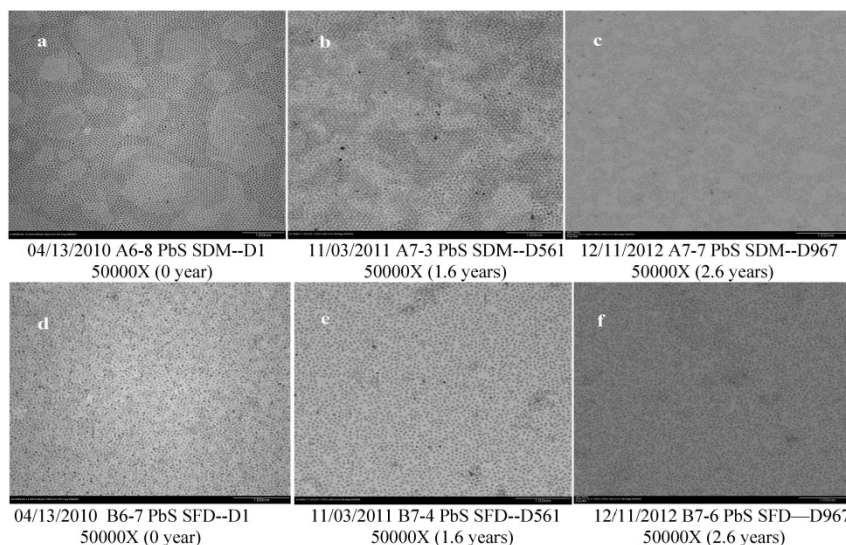


Figure 8. SDM (a,b,c) and scCO_2 (d,e,f) deposition of PbS on carbon coated copper grids, which were stored under ambient conditions about 2 years and 7 months. TEM images (a,d) were taken on Day 1, TEM images (b,e) were taken on Day 561, and TEM images (c, f) were taken on Day 967.

conditions. From observation of the TEM images, the QDs both oxidize and ripen in air and ripening occurs mostly by atomic diffusion between immobile QDs rather than by QD diffusion and aggregation. The edges of the QDs in Figures 8c and 8f became more faded than TEM images of Figures 8b and 8e, and those of Figures 8a and 8d.

4. CONCLUSIONS

The study presented here provides a detailed overview about the temporal impact of the ambient environment on the optical properties of PbS QDs, such as near infrared absorption and photoluminescence. The stability of the optical properties is of particular importance for optical device fabrication procedures and reliability. We observed changes in the optical properties over the time period of more than 4 months, for PbS QD films deposited from solution by both conventional solvent evaporation and solvent removal by a supercritical fluid CO_2 method. We also tested the samples

which remained under the ambient conditions for more than 2 years. The PbS QD films on GaAs and glass both had good adherence, despite the lack of a polymer matrix, and with the supercritical fluid CO₂ deposition process the films have a very uniform substrate coverage without the typical “coffee ring” pattern of standard solution deposition processes.

The optical data point towards slow oxidation of the QD surface despite the protecting oleic acid ligands. The lead oxide and sulfur oxide formation shrinks the active QD volumes, causing a blue shift of the emission and absorption. The absorption process is the more reliable method for tracking changes in the optical volume since it involves the transition between the two quantum confined states. Unfortunately, the emission process involves a transition between trap states and only one of the quantum confined states. The existence of traps in the investigated QDs is supported by the ~100 meV “Stokes” shift [33] between the initial absorption peak (951 meV) and the initial PL peak (858 meV). The oxide formation was confirmed using x-ray photoelectron spectroscopy.

The stability of the structural and optical properties of the unprotected QD films in ambient conditions is good over a time period of several months. The denser QD films formed by the SFD are more oxidation resistant than the films formed by the SDM method. Over a period of 4 months the QD optical absorption only shifted by 15 meV for the SFD processed films. This small shift reflects that only a small change in PbS QD active volume was occurred. For device fabrication the PbS QD layers would not remain unencapsulated and therefore would be even less likely to degrade over longer periods of time. A second PbS QD deposition to fill the micrometer or less cracks should take care of potential electrical continuity issues and testing of degradation of electrical properties needs to be done since these properties may degrade faster than the optical properties [18].

REFERENCES

- [1] Porter, V. J., Mentzel, T., Charpentier, S., Kastner, M. A. and Bawendi, M. G., “Temperature-, gate-, and photoinduced conductance of close-packed CdTe nanocrystal films,” *Phys. Rev. B*, 73, 155303 (2006).
- [2] Talapin, D. V. and Murray, C. B., “PbSe nanocrystal solids for n-and p-channel thin film field-effect transistors,” *Sci.* 310, 86–89 (2005).
- [3] Yu, D., Wang, C. J. and Guyot-Sionnest, P., “n-type conducting CdSe nanocrystal solids,” *Sci.* 300, 1277–1280 (2003).
- [4] Buda, M., Iordache, G., Stancu, V. and Botila, T., “Characterization of high performance PbS photodetectors,” *J. Optoelectronics and Adv. Mater.* 10 (2), 306–310 (2008).
- [5] Jarosz, M. V., Porter, V. J., Fisher, B. R., Kastner, M. A. and Bawendi, M. G., “Photoconductivity studies of treated CdSe quantum dot films exhibiting increased exciton ionization efficiency,” *Phys. Rev. B* 70, 195327 (2004).
- [6] Konstantatos, G., Howard, I., Fischer, A., Hoogland, S., Clifford, J., Klem, E., Levina, L. and Sargent, E. H., “Ultrasensitive solution-cast quantum dot photodetectors,” *Nature*, 442, 180–183 (2006).
- [7] Oertel, D. C., Bawendi, M. G., Arango, A. C. and Bulovic, V., “Photodetectors based on treated CdSe quantum-dot films,” *Appl. Phys. Lett.* 87, 213505-1-3 (2005).
- [8] Sun, L. F., Choi, J. J., Stachnik, D., Bartnik, A. C., Hyun, B. R., Malliaras, G. G., Hanrath, T. and Wise, F. W., “Bright infrared quantum-dot light-emitting diodes through inter-dot spacing control,” *Nature Nanotechnol.* 7, 369–373 (2012).
- [9] Bertoni, C., Gallardo, D., Dunn, S., Gaponik, N. and Eychmuller, A., Fabrication and characterization of red-emitting electroluminescent devices based on thiol-stabilized semiconductor nanocrystals,” *Appl. Phys. Lett.* 90, 034107 (2007).
- [10] Coe, S., Woo, W. K., Bawendi, M. and Bulovic, V., “Electroluminescence from single monolayers of nanocrystals in molecular organic devices,” *Nature*, 420, 800–803 (2002).
- [11] Plum, E., Fedotov, V. A., Kuo, P., Tsai, D. P. and Zheludev, N. I., “Towards the lasing spaser: controlling metamaterial optical response with semiconductor quantum dots,” *Optics Express*, 17(10), 8548–8551 (2009).
- [12] Shevchenko, E. V., Talapin, D. V., Kotov, N. A., O’Brien, S. and Murray, C. B., “Structural diversity in binary nanoparticle superlattices,” *Nature*, 439, 55–59 (2006).
- [13] Shevchenko, E. V., Talapin, D. V., Murray, C. B. and O’Brien, S., “Structural characterization of self-assembled multifunctional binary nanoparticle superlattices,” *J. Am. Chem. Soc.* 128, 3620–3637 (2006).

- [14] Zhao, N., Osedach, T. P., Chang, L. Y., Geyer, S. M., Wanger, D., Binda, M. T., Arango, A. C., Bawendi, M. G. and Bulovic, V., "Colloidal PbS quantum dot solar cells with high fill factor," *ACS Nano*, 4 (7), 3743–3752 (2010).
- [15] Gur, I., Fromer, N. A., Geier, M. L. and Alivisatos, A. P., "Air-stable all-inorganic nanocrystal solar cells processed from solution," *Sci.* 310, 462–465 (2005).
- [16] Dai, Q., Wang, Y. N., Zhang, Y., Li, X. B., Li, R. W., Zou, B., Seo, J. T., Wang, Y. D., Liu, M. H. and Yu, W. W., "Stability study of PbSe semiconductor nanocrystals over concentration, size, atmosphere, and light exposure," *Langmuir*, 25 (20), 12320–12324 (2009).
- [17] Sykora, M., Kuposov, A. Y., McGuire, J. A., Schulze, R. K., Tretiak, O., Pietryga, J. M. and Klimov, V. I., "Effect of air exposure on surface properties, electronic structure, and carrier relaxation in PbSe nanocrystals," *ACS Nano*, 4, 2021–2034 (2010).
- [18] Ihly, R., Tolentino, J., Liu, Y., Gibbs, M. and Law, M., "The photothermal stability of PbS quantum dot solids," *ACS Nano*, 5 (10), 8175–8186 (2011).
- [19] Stouwdam, J. W., Shan, J. N. and van Veggel, F. C. J. M., "Photostability of colloidal PbSe and PbSe/PbS Core/Shell Nanocrystals in solution and in the solid state," *J. Phys. Chem. C* 111 (3), 1086–1092 (2007).
- [20] Zhao, H., Chaker, M. and Ma, D., "Bimodal photoluminescence during the growth of PbS quantum dots," *J. Phys. Chem. C* 113, 6497–6504, (2009).
- [21] Hines, M. A. and Scholes, G. D., "Colloidal PbS nanocrystals with size-tunable near-infrared emission: Observation of post-synthesis self-narrowing of the particle size distribution," *Adv. Mater.* 15, 1844–1849, (2003).
- [22] Wang, J. S., Smetana, A. B., Boeckl, J. J., Brown, G. J. and Wai, C. M., "Depositing ordered arrays of metal sulfide nanoparticles in nanostructures using supercritical fluid carbon dioxide," *Langmuir*, 26(2), 1117–1123 (2010).
- [23] Smetana, A. B., Wang, J. S., Boeckl, J. J., Brown, G. J. and Wai, C. M., "Deposition of ordered arrays of gold and platinum nanoparticles with an adjustable particle size and interparticle spacing using supercritical CO₂," *J. Phys. Chem. C* 112, 2294–2297 (2008).
- [24] Liu, J., Anand, M. and Roberts, C. B., "Synthesis and extraction of β -D-glucose-stabilized Au nanoparticles processed into low-defect, wide-area thin films and ordered arrays using CO₂-expanded liquids," *Langmuir* 22, 3964–3971 (2006).
- [25] McLeod, M. C., Kitchens, C. L. and Roberts, C. B., "CO₂-expanded liquid deposition of ligand-stabilized nanoparticles as uniform, wide-area nanoparticle films," *Langmuir*, 21, 2414–2418 (2005).
- [26] Lin, X. M., Jaeger, H. M., Sorensen, C. M. and Klabunde, K. J., "Formation of long-range-ordered nanocrystal superlattices on silicon nitride substrates," *J. Phys. Chem. B* 105, 3353–3357 (2001).
- [27] Ohara, P. C. and Gelbart, W. M., "Interplay between hole instability and nanoparticle array formation in ultrathin liquid films," *Langmuir*, 14, 3418–3424 (1998).
- [28] Asunskis, D. J. and Hanley, L., "Valence band and core level x-ray photoelectron spectroscopy of lead sulfide nanoparticle-polymer composites," *Surf. Sci.* 601, 4648–4656 (2007).
- [29] Zachary, A. M., Bolotin, I. L., Asunskis, D. J., Wroble, A. T. and Hanley, L., "Cluster beam deposition of PbS nanocrystals into organic matrices," *ACS Applied Materials and Interfaces* 1(8), 1770–1777 (2009).
- [30] CasaXPS Version 2.3.15, Copyright © 1999–2009 Casa Software Ltd.
- [31] Moulder, J. F., Stickle, W. F., Sobol, P. E. and Bomben, K. D., "Handbook of x-ray photoelectron spectroscopy," copyright 1992, the Perkin-Elmer Corporation, USA.
- [32] Tarlov, M. J., Burgess, R. F. Jr., and Gillen, G., "UV photopatterning of alkanethiolate monolayers self assembled on gold and silver," *J. Am. Chem. Soc.*, 115, 5305 (1993).
- [33] Wang, J. S., Ullrich, B., and Brown, G. J., "Lead sulfide quantum dot synthesis, deposition, and temperature dependence studies of the Stokes shift," 2011 MRS fall proceeding, Mater. Res. Soc. Symp. Proc. Vol. 1409 2012 Materials Research Society DOI:10.1557/opl.2012.755.

LIST OF ACRONYMS, ABBREVIATIONS, AND SYMBOLS

<u>Acronym</u>	<u>Description</u>
PbS	Lead Sulfide
QDs	Quantum Dots
PL	Photoluminescence
TR	Transmittance
FTIR	Fourier Transform Infrared
FRET	Fluorescence Resonance Energy Transfer
Sc-CO ₂	Supercritical Fluid Carbon Dioxide
TEM	Transmission Electron Microscopy
2D	Two-Dimensional
HRTEM	High Resolution Transmission Electron Microscopy
XRD	X-ray Diffraction
fcc	Face-centered-cubic
SEM	Scanning Electron Microscopy
ODE	Octadecene
TMS	Bis(trimethylsilyl)sulfide
TOP	Trioctylphosphine
OA	Oleic Acid
GAS	Gas-Antisolvent
FEG	Field Emission Gun
OA	Optical Absorbance
cw	Continuous Wave
NPs	Nanoparticles
PINCs	Production of Polymer-Inorganic Nanocomposites
PET	Polyethylene Terephthalate
CDM	Centrifuge Deposition Method
FWHM	Full-Width at Half Maximum
LO	Longitudinal Optical
XPS	X-Ray Photoelectron Spectroscopy
AFM	Atomic Force Microscopy
SFD	Supercritical Fluid Deposition
SDM	Solvent Deposition Method
S.I.	Semi-Insulating
G/L	Gaussian/Lorentzian